View metadata, citation and similar papers at core.ac.uk
brought to you by CORE
provided by Universidade do Minho: RepositoriUM

BOND OF NSM FRP STRENGHTENED CONCRETE: ROUND ROBIN TEST INITIATIVE

Bilotta A.[1], Ceroni F.[2], Barros J.A.O. [3], Costa I.[4], Palmieri A.[5], Szabo K.Z.[6], Nigro E.[7], Matthys S.[8], Balazs G.L.[9], Pecce M.[10]

[1]Ph.D, postdoctoral research associate, University of Naples, Department of Structural Engineering, Via Claudio 21, 80125, Naples, Italy, antonio.bilotta@unina.it

[2]Ph.D, Assistant Professor, University of Sannio Engineering Department, Piazza Roma 21, 82100, Benevento, Italy, ceroni@unisannio.it, corresponding author

[3]Ph.D, Full Professor, University of Minho ISISE, School of Eng.,University of Minho, Campus de Azurem, 4800-058, Guimaraes, Portugal, barros@civil.uminho.pt

[4]Ph.D, postdoctoral research associate, University of Minho ISISE, School of Eng.,University of Minho, Campus de Azurem, 4800-058, Guimaraes, Portugal, ines.costa@civil.uminho.pt

[5]PhD., Ghent University, Magnel Laboratory for Concrete Research, Technologiepark-Zwijnaarde 904, B-9052 Gent, Belgium, palmieri.aniello@gmail.com

[6]Ph.D, Budapest University of Technology and Economics, Department of Construction Materials and Engineering Geology, Muegyetem 3, Budapest, H-1111, Hungary, zsomborus@yahoo.com

[7]Ph.D, Associate Professor, University of Naples, Department of Structural Engineering, Via Claudio 21, 80125, Naples, Italy, emidio.nigro@unina.it

[8]Ph.D, Associate Professor, Ghent University, Magnel Laboratory for Concrete Research, Technologiepark-Zwijnaarde 904, B-9052 Gent, Belgium, Stijn.Matthys@ugent.be

[9]Ph.D, Full Professor, University of Technology and Economics, Department of Construction Materials and Engineering Geology, Muegyetem 3, Budapest, H-1111, Hungary, balazs@vbt.bme.hu

[10]Ph.D, Full Professor, University of Sannio, Engineering Department, Piazza Roma 21, 82100, Benevento, Italy pecce@unisannio.it

Abstract

Despite the extensive research that has been conducted on the debonding behaviour of FRP strengthening systems, no standard methodology has been yet established on its experimental characterization. In this context, to assess the performance and reliability of small scale testing on NSM (near surface mounted) FRP strengthening systems, an experimental program was carried out on a series of nine NSM FRP strengthening systems, in the framework of an international Round Robin Testing (RRT). Eleven laboratories and seven manufacturers and suppliers participated in this extensive international exercise, which regarded both NSM and EBR FRP strengthening systems. Test results obtained for the NSM systems by the participating laboratories are discussed and compared in this paper to investigate the feasibility of the adopted single/double pulling shear test method, to investigate the mechanism of bond between NSM FRP reinforcement and concrete, and to investigate the level of variability obtained between the participating laboratories testing the same material batches.

It is concluded that the tested variants in the adopted single/double shear pulling test have a significant influence, stressing the importance of the level of detail of standardized test protocols for bond verification. On overall, given the variants included in this study, the obtained variation in bond stress-slip behaviour between the laboratories remained fairly limited.

Keywords: Near Surface Mounted technique, FRP materials, Bond test, Round Robin Testing, Bond behaviour, Debonding.

Introduction

In recent years, strengthening technologies for reinforced concrete structures using FRP composites have been gaining widespread interest and growing acceptance in the civil engineering industry. The EBR (external bonded reinforcement) and the NSM (near surface mounted) are the most common strengthening techniques. The EBR consists of bonding, with a high strength adhesive, a laminate/textile onto the surface of the concrete element, while the NSM consists of placing FRP reinforcing bars into grooves pre-cut on the concrete members and embedding them with a high strength adhesive. The main property governing the design of a FRP strengthening application is the debonding of the FRP, which is generally initiated before the tensile strength of the FRP reinforcement is reached. For this reason, some of the first investigations on the topic have specifically addressed the issue of bond using different test methods (De Lorenzis et al. 2002, Blaschko 2003, Hassan and Rizkalla 2003, De Lorenzis et al. 2004, Kotyinia 2005, Seracino et al. 2007) both for EBR and NSM techniques, but usually aiming to simulate the pull-out of the FRP material. The different types of pull-out tests can be grouped in the following general categories (Chen et al. 2001): single/double-shear pushing test, single/double-shear pulling test, and beam bending test (see **Figure 1**). In order to produce representative small scale testing procedures, it is necessary to understand the mechanisms that trigger the pull-out of the FRP. For that purpose, **Figure 2** exemplifies the effective stress state installed in a flexural and shear FRP strengthening, as well as in the surrounding steel reinforcement (Costa and Barros 2013). In fact, it is perceptible that the FRP pull-out mechanism typically occurs in a zone where the concrete is loaded in tension and the local pull-out is initiated due to crack opening. Taking as example the detail of the flexural crack, not only the concrete is loaded in tension, but also the adjacent steel reinforcement. The same occurs for the case of the shear strengthening, since all intervening materials experience tension.

Regarding the loading configurations commonly applied (in **Figure 1**), none of them is able of reproducing accurately the real behaviour of the composite reinforcement when applied to a real structural member (in **Figure 2**).

Of all the configurations given in **Figure** 1 (Ueda and Dai, 2005; De Lorenzis and Nanni, 2001; Horiguchi and Saeki, 1997), the shear pulling test are the ones that more resemble the real stress conditions of the different reinforcement systems. In fact, the applied forces in the external FRP reinforcement and the internal steel bars to pull the specimen, have opposite directions. As a result the concrete is subjected to tension, which does not provide unrealistic favourable confinement to the FRP.

On the one hand, shear pushing tests can introduce a compressive stress field in the concrete surrounding the bond length, which can promote a confinement action to the FRP. In case the compressive stress field is limited and is quite distant from the FRP reinforcement-concrete interface, this effect becomes negligible. On the other hand, beam bending tests may introduce large flexural effects in the FRP reinforcement, given the curvature in the cross-section of these specimens. These flexural effects tend to be higher than observed in FRP-flexural strengthened RC beams.

However, the objective of these relatively small scale models is not only the determination of bond behaviour in terms of failure load, strain distribution and slip values, but also the possibility to assess the relative efficiency of various FRP strengthening systems. In the specific case of this RRT, it is also used to verify possible differences when tests are carried out in different laboratories.

The bond performance of NSM FRP, however, has yet to be fully addressed, and is a key area requiring further research. In this scope, a round robin testing (RRT) initiative was conducted to investigate: (1) the bond mechanism between the NSM FRP reinforcement and the concrete, comparative for different material systems; (2) the influence of different variants of the adopted single/double-shear pulling test; (3) possible differences when a test protocol is carried out in different laboratories on the same material batch; and (4) the influence of variations in concrete strength following differences in constituent materials between countries in applying a prescribed mix.

To this aim eleven laboratories and seven manufacturers and suppliers participated in this extensive international exercise, which regarded the characterization of both mechanical properties and bond behaviour of NSM and EBR FRP systems and was carried out within the framework of the European funded Marie Curie Research Training Network, EN-CORE, with the support of Task Group 9.3 of the International Federation for Structural Concrete (*fib*). Four laboratories participated in the RRT on the bond behaviour of NSM FRP strengthening system (see **Table 1**). The proposed bond test methods are analysed and discussed along the paper, evidencing their positive and negative aspects. Some of the factors expected to affect the bond performance are addressed, namely the type of FRP material, FRP cross section, shape and surface configuration of the FRP bar/strip. The test results obtained by the participating laboratories are discussed and compared in this paper in terms of both global (failure modes and loads) and local behaviour (distribution of axial strain along the FRP reinforcement and shear stress along the interfaces).

Experimental investigation

Test Specimen and Parameters

The experimental program has been carried out using 9 different NSM FRP strengthening systems for a total of 94 tests, with a minimum of 2 tests per strengthening system at each laboratory, even if generally 3 tests were performed for each type of NSM system. As such, suppliers were asked to ship testing materials from the same production batch to the different testing laboratories. Two different test setup methodologies, namely a double bond shear-pulling test (DB), and a single bond shear-pulling test (SB) have been adopted by the participating laboratories as shown in **Figure 3**. In both schemes the concrete is loaded in tension by means of steel bars embedded in the concrete block, so that both the steel bars and the concrete block are loaded in tension. All tests were carried out using universal testing machines.

In all schemes the FRP bars/strips were bonded to the concrete prism for a length of 300 mm (L_b), whilst a 50 mm long region was left unbonded at the loaded end to prevent the development of high shear stresses and avoid premature local damage on the concrete. This bond length has been chosen on the basis of experimental data in literature (among which Sena-Cruz et al., 2004; and Seracino et al., 2007) and in due consideration that the total specimen length should comply clearance in tensile testing machines. Grooves were saw-cut in the hardened concrete specimens and application of FRP reinforcements was done as specified by the manufacturers

The DB specimens were composed of two concrete blocks (400×150×150mm^3) connected only by means of two identical FRP bars, bonded in opposite faces of the concrete blocks. Each of the concrete blocks had two 16 mm steel bars with an embedment length of 380 mm (only one bar with diameter 22 mm in the case of Budapest laboratory), responsible for ensuring the load transference from the concrete blocks to the FRP bars, and the necessary anchorage to the universal testing machine.

To prevent debonding in the not instrumented half of the specimen, the bond length is taken somewhat longer than 300 mm and optionally an extra clamp has been provided (in Ghent, see **Figure 3a**; and in Minho, see **Figure 3c**). Given concerns of concrete splitting cracks along the plane formed by the internal steel bars, at Minho an extra clamp was provided at the extremity of the test region (Fig. 3c). The shaped clamp had no contact with the FRP strengthening zone and had minimal torque, so to not significantly disturb the strain/stress field in the bond region.

The bond tests according to the SB setup were carried out on one concrete prism (400×200×160mm^3) in a servo-hydraulic testing machine (**Figure 3d**). Steel pipes or tabs were installed at the end of the FRP reinforcement in order to ensure adequate clamping in the grips of the testing machine. The specimen was blocked at the lower base of the testing machine by means of two steel bars (diameter 20 mm) embedded in the concrete prism, and bolted to a system of steel plates fixed in the lower grips. The NSM reinforcement was applied on both sides of each concrete block, but each side was tested separately, so that the test was a single shear test.

Strain gauges (SGs) were applied on the NSM reinforcement to measure strain, and one or two LVDTs were used to measure the relative displacement between the reinforcement and the concrete. In particular, in the DB tests carried out at Ghent and Budapest laboratories 5 SGs at a distance of 10 mm, 80 mm, 150 mm, 220 mm and 290 mm from the beginning of the bonded zone were glued on the reinforcements of both monitored sides (see **Figure 3a and 3b**). Analogously, in the SB test of Naples/Sannio laboratory 5 SGs were applied according to the same configuration on the FRP reinforcement.

In the DB tests of Minho laboratory, only 3 SGs at a distance of 10 mm, 80 mm, and 220 mm from the beginning of the bonded zone were glued on only one side of the NSM FRP reinforcement (see **Figure 3c**).

In all cases, for installing the SG, the surface of the FRP was scraped/sanded to expose the core zone. Strain gauges have been adhered to the FRP surface and where covered with a protective layer, so to guarantee that no interaction between the strain gauge and surrounding fresh and hardened epoxy would occur.

All tests were conducted under displacement control with displacement rates of 0.1 mm/min to 0.5 mm/min. The recommended loading rate of 0.1 mm/min deviated between laboratories given the available equipment, but remained in the same order of magnitude. The loading rates were sufficiently low to be considered of limited influence on the failure aspect and bond failure loads, as could be observed from the obtained test results. **Table 1** summarizes the main procedural differences between testing laboratories.

The influence of the FRP reinforcement shape (bars versus strips), the type of fibres, as well as the type of surface treatment were evaluated in the RRT. An overview of the different types of NSM FRP reinforcements is given in **Table 2**. The FRP reinforcements are listed using the following designation: the first letter C, B, or G indicates Carbon, Basalt or Glass fibres, respectively; the second notation indicates the surface treatment, SC = Sand Coating, RB = Ribbed Bars, S = Smooth bars or strips, and SW = Spirally Wounded bars (see **Figure 4**); finally, the third notation indicates the dimension of the bar/strip reinforcement (diameter for the bars or thickness and width for the strips). Three specimens were tested for each type of NSM reinforcement system.

Materials

A target concrete strength of 30 MPa, with a predefined reference concrete mix (gravel 4/14: 1250 kg/m³, coarse Sand: 665 kg/m³, CEM I 42,5: 300 kg/m³, water: 170 kg/m³) was applied for the RRT. Given different constituent materials available in the participating countries (Belgium, Italy, Portugal, Hungary), a variation in compressive cylinder strength has been observed as indicated in **Table** 1. Given this observation, the concrete strength variability was considered as an additional variable as part of this RRT initiative.

The average values of the mean compressive cylinder (diameter of 150 mm and a height of 300 mm) and cubic strength (side length of 150 mm), $f_{cm,cyl}$, and $f_{cm,cub}$, the mean tensile strength obtained by bending tests (150 mm×150mm×600mm with a span length of 50 mm), $f_{ctm,flex}$, and the secant Young's modulus, E_c, are summarized in **Table 1**. All results were obtained by experimental tests on at least three specimens tested 28 days from casting and, in some cases, also at the time of the bond tests. The average value of E_c was obtained in the cylinder specimens used for the compressive strength. Moreover, from Brazilian tests with 3 cylinder specimens of 150 mm diameter × 300 mm height, the Naples/Sannio laboratory obtained an average indirect tensile strength of 2.5 MPa at the age of testing.

The tensile properties of the NSM FRP reinforcement were obtained by different laboratories on three to five specimens. In **Table 3**, the average values of tensile strength, f_f, modulus of elasticity, E_f, computed in relation to stresses in the range of 20-50% (ISO TC 71/SC 6 N) by Ghent laboratory or of 20-60% (ACI 440.3R) by Naples/Sannio and Minho laboratories, and ultimate failure strain, ε_{fu}, are listed for each participating laboratory. The nominal cross-sectional area of the FRP furnished by the producers has been used for calculating the experimental values of tensile strength and modulus of elasticity.

Finally, **Table 4** reports the average tensile strength and modulus of elasticity considering all the tests, along with the correspondent CoV values, cross sectional area, A_f, and axial stiffness, $E_f{\cdot}A_f$.

As very similar testing protocols have been used for FRP tensile testing by the laboratories (following ISO 527-5/ASTM D3039), it is interesting to note the obtained CoV's. In terms of modulus of elasticity limited variation is obtained, with a CoV in the range 1 to 11%. In terms of tensile strength however, much larger variation is obtained with a CoV between 5 to 36%. Also, looking to the CoV of the individual laboratories, much higher variations are observed for tensile strength than for modulus of elasticity. These results can also be noted from the ratio's ($f_{u,exp}/f_{u,nom}$) and ($E_{f,exp}/E_{f,nom}$) in **Table 4**, and confirm the sensitivity of FRP tensile testing in terms of strength to the anchorage detailing, as also stated by the test standards.

The higher variability of the tensile strength is evident also in the results of the single laboratory: the CoV of average tensile strength is, indeed, always higher than the CoV of Young's modulus. The CoV further increases when the average values are calculated considering the results of different laboratories. The worst result is represented by the carbon strip C_S_2.5x15, where the high stiffness and the shape have probably contributed to make not perfect the anchorage of the coupons in the grips. It is worth to note the results obtained by the Naples/Sannio laboratory are characterized by the lowest scatter both in terms of Young's modulus and tensile strength.

All the NSM FRP reinforcements were embedded into the grooves by means of the appropriate epoxy resin suggested by the manufacturers. Tests on adhesive samples were also carried out by the Minho laboratory and the obtained results, in terms of tensile strength, f_a, and elastic modulus, E_a, are given in **Table 5**.

Experimental results and discussion

Failure modes and ultimate loads

The pull-out behaviour of a NSM system is assumed as a successive balance of strength between concrete fracture, debonding and rupture of the NSM system. Often, during the pull-out tests, a sequence of different failure modes was visible. In particular, when the debonding pull-out force is higher than the concrete fracture resistance, concrete fracture propagation is initially the dominant failure mode. However, the successive cracking of concrete along the interface results in a decrease of the bonded length. After this occurrence, the typical debonding failure mode takes over, and the fracture of a small volume of concrete surrounding the NSM system is generally observed. To simplify the analysis of the results, the experimentally observed failure aspects (FA) were categorized as follows, and the dominant failure mode was assigned to each specimens (see **Tables 6 and 7**):

- Debonding at the FRP-adhesive interface (DB-FRP/A)
- Debonding at the concrete-adhesive interface, with various degrees of concrete damage (DB-C/A)
- Adhesive splitting failure (SP-A)
- Tensile failure of the FRP (T-FRP)
- Splitting failure of the concrete along the plane of the internal steel bars (SP-C)

In the pull-out tests executed, several of these types of failure modes were observed. The most frequently observed resulted from the debonding at the concrete/epoxy interface (DB-C/A), with varying degrees of concrete damage (see **Figure 5b**) or a cohesive failure in the adhesive (epoxy splitting, SP-A, see **Figure 5c**). Only in few cases (bar C_S_8 tested by Ghent Laboratory and bar G_SW_8 tested by Naples/Sannio laboratory), a failure at the reinforcement/epoxy interfaces occurred with slipping of the bars respect to the surrounding concrete (DB-FRP/A, see **Figure 5a**).

Other types of failure, not related to debonding phenomena, but to the concrete strength were also observed: in particular, for a small percentage of the specimens the stress development along the embedded steel bars in addition to the stresses into the concrete (induced by the FRP reinforcement bars) have caused a premature failure of the concrete specimen by splitting (SP-C, see **Figure 5d**) or extensive concrete fracture. Finally, for the strip C-S-1.4x10 a tensile rupture of the fibres (T-FRP, see **Figure 5e**) was observed in the tests at Naples/Sannio laboratory.

Since the first three failure modes are all caused by the 'debonding' phenomena, in **Tables 6 and 7** only the results of the specimens failed for debonding (DB-FRP/A, DB-C/A, SP-A) are reported.

The average values of the debonding load considering the results of all laboratories and the corresponding CoV are also listed in **Table 8**. The results achieved in the Naples/Sannio and Budapest laboratory are very low scattered (maximum CoV of about 10%), followed by the ones obtained at the laboratories of Minho and Ghent University, which in some cases attained CoV of about 15%. This higher scatter can be due to the double shear test configuration, which is sensitive to proper alignment of the internal steel rebars as well as the NSM reinforcement. Furthermore, some inherent eccentricities during testing cannot be avoided given small material variations between the two simultaneous tested bond interfaces.

Looking to the values of CoV referring to the average maximum loads calculated considering the results of all laboratories (see **Table 8**), it can be observed that they vary in the range 6-16%. Considering the variability of concrete strength (23 MPa for SB and 32-42 MPa for DB) and the differences in applied testing details between the laboratories, this obtained range of CoV can be regarded acceptable.

On the other hand, results of Budapest are generally lower than the other laboratories, despite their higher concrete strength ($f_{cm,cub}$ = 42 MPa). To verify this aspect and to isolate the influence of the differences in test procedure, considering the variants in concrete strength, in

Figure 6 the average failure loads obtained by each laboratory are normalized with respect to the square root of the compressive strength as usually considered in debonding models for EBR systemsr. Therefore the parameter $\mu = \dfrac{F_{u,av}}{\sqrt{f_{cm,cyl}}}$ is defined and plotted in **Figure** 6a. Note that a lower exponent is expected for NSM systems (Seracino et al., 2007), but further bond tests are needed to assess in detail the effect of concrete strength on the failure loads and modes. The reduced effect of the concrete was also evidenced in an regression analyses carried out by Bilotta et al. (2014) on the results of the RRT initiative and on other results of bond tests collected in the technical literature.

From **Figure 6** the following is observed. The lowest results are obtained by Budapest, who used a DST with a single rebar to tension the concrete. Comparable results are obtained between Gent and Minho, since they had almost identical test configuration and similar concrete strength. Some differences in results between these 2 labs remain however. This means that the procedure to realize a DST is less stable to warrant the same results in different laboratories. The highest results are obtained by Naples/Sannio who adopted a single shear test-up version and had the lowest concrete strength.

Table 9 lists the results of specimens that failed due to concrete splitting or concrete fracture (SP-C), while **Table 10** reports the tests where the tensile rupture of the fibres occurred (T-FRP).

It is worth to notice that for the square carbon bar C_S_10x10, failure was often due to concrete splitting along the internal rebars (SP-C). This undesired specimen failure indicates that the test configuration appeared not functional for the complete range of tested FRP material systems and bond failure at the internal rebars was predominant over that of the C_S_10x10.

For the carbon strip C_S_1.4x10 the tensile rupture of the fibres (T-FRP) was achieved in all tests carried out at Naples/Sannio laboratory at an average value of 32.9 kN (that corresponds to an average tensile stress of 2350 MPa), while at laboratory of Minho a debonding failure

(DB-C/A) was achieved at higher loads (39.1 kN, that corresponds to a tensile stress of 2793 MPa) and at Ghent and Budapest laboratories a concrete failure occurred at lower loads (about 25 kN). However, it is worth to mention that according to **Table 3**, the experimental average tensile strength of the strip C_S_1.4x10 was 2221 MPa for the Naples/Sannio laboratory and 3047 MPa for the Minho laboratory. Such a difference in the tensile strength might be a reasonable explanation also for the difference of the failure loads and modes attained in the pull-out tests by these two laboratories.

Also for one specimen strengthened with B_SC_6 bar a tensile rupture of the bar occurred in the test carried out by Naples/Sannio laboratory; the maximum tensile stress achieved for such a bar (1215 MPa) was, indeed, comparable with its tensile strength (see **Table 3**).

In **Figure 7a**, the average values of the maximum strain, $\varepsilon_{\max} = F_u / \left(A_f . E_f \right)$, are plotted versus the axial stiffness of the FRP NSM reinforcements. This figure shows that the maximum strain decreases with the axial stiffness of the FRP reinforcement according to a decreasing trend that is typically observed also in EBR systems. The graph shows that the maximum strain was about 2% in the case of 6 mm basalt bars, but most bars and strips attained maximum strains in the range 0.6-1.5%, and the lowest strain was about 0.35%. Note that for EBR plates the maximum strain at debonding is usually about 0.2% (Bilotta et al. 2011, Guadagnini et al. 2012).

In **Figure 7b** the average values of failure loads in case of debonding failure are plotted versus the axial stiffness of the reinforcement. This graph shows a tendency for the failure load to increase with the axial stiffness, especially for values of the axial stiffness lower than 7 10^6 MPa mm^2. The carbon bar C_SC_6 represents a singular result, since, despite its relevant stiffness ($E_f A_f$ = 5.21 10^6 MPa mm^2), the maximum load achieved is rather lower than the trend observable in the graph. This is likely due to the surface texture of this bar (sand coated). Indeed, differences in FRP surface texture can be expected to influence the observed trend between failure load and axial stiffness).

These results seem to confirm again that the concrete strength has no evident influence on the maximum strain or the maximum load, but that a meaningful parameter is the axial stiffness of the FRP NSM reinforcement. This statement is supported by Ceroni et al. (2012), where a larger database of bond tests on different types of NSM systems was collected in terms of maximum load and, thus, maximum strain at failure. According to these authors, no clear influence of the concrete strength was individuated. On the contrary, the effect of the surface treatment can be observed looking to the results of bars B_SC_8, G_RB_8, G_SW_8 characterized by the same diameter (8 mm) and similar elastic modulus (in the range 49-61 GPa), but different surface treatment. In particular, the glass bar with ribbed surface failed for the highest load (46 kN), followed by the spirally wound glass bar (42 kN) and the sand-coated basalt bar (34 kN). Moreover, the shape of the NSM system can have influence on the bond strength, since the specimens strengthened with the smaller strip C_S_1.4x10, despite having axial stiffness in the same range of the value of bars B_SC_8 and G_SW_8, nevertheless the smooth surface, attained a load comparable with the ribbed bar G_SW_8 (39.1 vs. 41.6 kN).

To investigate more in detail the effect of the shape factor of the FRP, which can be defined as the ratio between the perimeter and the cross sectional area of the FRP, in **Figure 7c** the maximum tensile stress is plotted versus the shape factor. It can be observed that this stress is directly proportional to the shape factor and that, in particular, the carbon strips, characterized by larger shape factor, attained higher tensile stresses at failure. This result is applicable as long as an adequate bond quality and bond length are provided, meaning that for very small bond lengths this might not be valid.

Load-displacement curves

The load versus loaded end slip, *P-s,* of the different NSM systems tested by the four laboratories is compared in **Figure 8**. Such *P-s* relationships were obtained as the average curves of the three tests carried out by each laboratory on equal specimens.

The slip between the FRP reinforcement and the concrete, *s*, was obtained by integrating the strain along the bonded length. The displacement measurements recorded by the LVDTs were not capable of providing directly this slip for the reasons exposed in Costa and Barros (2013). Assuming that the slip at the unloaded end can be considered negligible before debonding, and neglecting strain in the concrete, the slip was calculated through the following equation:

$$s=\sum_{k=1}^{n}\left(\varepsilon_k+\varepsilon_{k+1}\right)\cdot\frac{\Delta x_k}{2} \tag{1}$$

where ε_k and ε_{k+1} are the strains measured by SGs k and k+1, n is the number of strain measurements along the bond length, Δx_k is the distance between two consecutive SGs (Δx_k=70 mm or 140 mm).

In spite of the fact that the tests have been carried out by different laboratories, using concrete of different strength class, where equal testing conditions are almost impossible to assure, the results presented in **Figure 8** evidence that the average *P*-*s* curves obtained by the laboratories were, in general, very similar, except for single outliers in for example **Figure** 8(d) and 8(f), and which can be attributed to some testing difficulties experienced by the laboratories. It is also remarkable that in case of Minho, the loaded end slip was similar to the one obtained by the other laboratories, even though it was obtained using the strain values recorded in three SGs, while in the other laboratories five SGs were used.

Local behaviour

Distribution of strain

In order to compare the strain field in the bond length, the strain distributions are compared in **Figure 9** for all the NSM systems tested at two load levels corresponding to about 20-30% and 60-70% of the average maximum load. In all cases, the strain at z = 0 was calculated based on the magnitude of the applied load divided to the average values of the axial stiffness of the examined NSM system (see **Table** 4).

In general, for the different selected load levels, the strain distribution along the bond length was comparable between laboratories. It is worth mentioning that in the case of B_SC_8, the specimens tested at Minho exhibited a higher strain profile at 25 kN, as already **Figure 8b** had suggested, when a progressive loss of stiffness was initiated at about 15 kN.

Additionally, regarding C_S_1.4x10, it is interesting to observe that the strain profile of the specimens tested at Budapest, at 25 kN, clearly show that debonding is on the verge of occurring. Note that according to **Table 9**, the average failure load of these specimens was 25.1 kN.

Bond stress – slip relationship

Bond stresses were determined by utilizing experimentally recorded strains along the FRP. Referring to two consecutive SGs, spaced of Δx_i= 70 mm (or 70 mm and 140 mm in the case of the specimens tested in Minho laboratory), and assuming uniform distribution of the bond stress in this interval, bond stresses are obtained from the following equilibrium equation:

$$\tau_x = E_f \cdot \frac{A_f}{p_f} \cdot \frac{\Delta\varepsilon_i}{\Delta x_i} \tag{2}$$

where $\Delta\varepsilon_i$ and Δx_i are the strain difference and the distance between the two considered SGs. The other parameters of equation (2) were already defined.

The bond stress-slip (τ–s) relationship is obtained considering Eq. (1) for calculating the slip and the measurements of the first two strain gauges for calculating the shear stress close to the loaded end of the reinforcement.

The bond stress-slip relationships of the tested specimens are given in **Figure 10**. For each laboratory, such curves are the average ones of the tested specimens strengthened with the same NSM system, as already done for the P-s curves. From **Figure 10**, the repeatability of the test results among the participating laboratories is notorious for similar types of failure mode, despite the different test setups. Note that, since the shear stress has been evaluated by using the measures of the first two bonded strain gauges, the bond law is always completely developed for whatever failure modes.

On overall a more or less bilinear behaviour is observed, with some degree of plateau in the region of maximum bond stress. This plateau is less pronounced than sometimes suggested in literature (eg. De Lorenzis and Teng, 2007). Indeed, the post-peak branch of the experimental bond stress-slip behaviour is sensitive to higher uncertainty, since the cracking of the bonded surface is in an advanced status and the strain gauges can give anomalous measures due to local damages. For this reason, experimental observations on the shape of the bond law can be further complemented by numerical analysis (Ceroni et al., 2013).

Note that the results reported by Minho for the strip C_S_1.4x10 (Fig. 10f) show a higher bond strength compared with the remaining laboratories, since a real debonding failure occurred in the tests of Minho (**Figure 5b**), while in the others laboratories a tensile failure of the strip or concrete splitting occurred at lower loads, as previously discussed.

In **Figure 11**, a comparison of the experimental τ-s curves obtained for all the tested NSM systems is reported. For each NSM system an average curve has been plotted considering the results of all the laboratories that have tested the considered NSM system. Since the graph shows that the local bond stress slip relationship can be reasonably approximated by a bilinear diagram identified by the following parameters: peak shear stress, τ_{max}, corresponding slip, s_{el}, and ultimate slip, s_u, that can be assessed by extrapolating the post peak softening branch of the experimental τ-s curves However, it is worth to note the after-peak branch is affected by more uncertainness since the cracking of the bonded surface is in an advanced status and the strain gauges can give anomalous measures due to local damages. Therefore, as in most cases the brittle behavior of concrete governs failure, it is not possible to witness the potential plateau that some authors in literature refer (De Lorenzis and Teng, 2007). An attempt to better assess the shape of the bond law and, i.e., verify the presence of a residual shear stress, have been done by means of numerical analyses in (Ceroni et al., 2013).

The above mentioned parameters of the experimental bond law are different as the axial stiffness and the shape of the NSM reinforcement change. In particular, the 8 mm diameter ribbed glass bars (G_RB_8) and the 6 mm diameter sand coated basalt bars (B_SC_6) reach the highest values of the peak shear stress and also of the ultimate slip. The ribbed configuration of the surface of the glass bars and the sand coating of the basalt ones should indicate that the ultimate slip can increase with the roughness of the surface of the FRP reinforcements, resulting in an increase of the energy absorption capacity. Even so, it is worth to note that this result is also influenced by the lower axial stiffness of these bars compared to the other reinforcements.

Lower values of both shear stress and ultimate slip are, indeed, attained by the 8 mm sand coated basalt bars (B_SC_8) and the thinner carbons strips (C_S_1.4x10), even if the slope of the softening branch is similar. On the contrary, for the other CFRP reinforcements, the values of the peak shear stress and of the ultimate slip are lower and the slope of the softening branch is larger, evidencing, thus, a more pronounced post-peak bond stress decay. The average experimental curves reported in **Figure 11** evidence that both the peak shear stress and the ultimate slip increase with the decrease of the axial stiffness of the NSM reinforcement and the elastic stiffness of the bond law increases as the axial stiffness is greater. These outcomes have been already highlighted in the numerical analysis developed on the results obtained by Naples/Sannio and Minho laboratories (Ceroni et al. 2012, Ceroni et al. 2013).

The effect of the axial stiffness is also visible looking only to the behavior of the carbon NSM systems, even if the strips seem to be lightly disadvantageous in terms of maximum shear stress compared with the round bars with similar axial stiffness (i.e. see the bond slip of C_S_2.5x15 and of C_S_8).

The effect of the surface texture is not always clearly identifiable based on the results of the tests carried out within this RRT initiative, since it is mixed with the effect of the different axial stiffness of the tested NSM systems. The influence of the surface texture can for example be observed, when comparing diameter 8 mm specimens G_RB_8 and B_SC_8 in **Figure 11**. The

G_RB_8 specimens obtained larger values of τ_{max}, and s_u, despite their 20% higher axial stiffness (in contradiction to the observed inversed proportionality between the peak bond stress point and the axial stiffness for most of the specimens). This is likely due to the distinct difference in surface texture between this ribbed GFRP bar and sand coated BFRP bar.

The different surface treatment is expected to be reflected also on the post-peak behaviour since it is, in general, more brittle in case of a smooth surface when compared to a ribbed one, due to the rapid decay of bond since the interlocking phenomena are less pronounced. Both basalt and glass bars show, indeed, sensibly higher ultimate slip and lower slope of the softening branch compared to the smooth carbon NSM systems.

Conclusions

A Round Robin Testing (RRT) initiative was conducted to investigate the feasibility of the adopted single/double pulling shear test method, to investigate the mechanism of bond between NSM FRP reinforcement and concrete, and to investigate the level of variability obtained between the participating laboratories testing the same material batches. Different laboratories and seven manufacturers and suppliers participated in this extensive international exercise, which was initiated within the framework of the European funded Marie Curie Research Training Network, EN-CORE, with the support of Task Group 9.3 of the International Federation for Structural Concrete (*fib*).

Two test setup variants, an asymmetrical pull-pull setup (single bond test, SB) and a symmetrical pull-pull setup (double bond test, DB) were adopted with concrete specimens of target compressive strength of 30 MPa. Variations in constituent materials of the concrete (with prescribed composition) in the different countries resulted in variations in the concrete strength between 23 and 49 MPa, which contributed to the obtained variations in the test results. Though the influence of the concrete strength was demonstrated to be limited, it could not be completely neglected and bond strength results were normalized with respect to the square root of the compressive strength.

Internal steel bars were used to transfer the tensile load to the DB specimens, which in some cases promoted the occurrence of premature specimen failure due to concrete splitting. Moreover, the detailing of the internal steel bars seems to have an indirect influence on the obtained bond strength results and requires precise test descriptions to be followed. These are negative aspects of this pulling shear test configuration, despite its strait forwardness as a possible standard test method.

Comparing the SB and DB variants, the latter yielded systematically bond strength values which were slightly lower (about NN%). Though the test description aimed in minimizing eccentricities, parasitic flexural effects of the DB configuration remained significant when considering the obtained coefficients of variations. Nevertheless, a comparison in terms of bond stress-slip curves seems to give a good agreement between the participating laboratories and different test setups for similar failure aspect. The maximum failure load and the bond strength varied with the type of reinforcement. However, debonding at the concrete/epoxy interface, with varying degrees of concrete damage, was the predominant observed failure aspect. Observed influence of the concrete strength or test setup on the bond behaviour remained limited to small, whereas obtained results were mainly dependent on the axial stiffness and the surface texture of the NSM systems. In particular, for the tested FRP NSM reinforcements, it was observed that the failure load increases: 1) as the axial stiffness increases until a certain value (about 7 10^6 MPa mm^2), and 2) for NSM systems characterized by similar axial stiffness, the ribbed surface allowed to transfer higher loads compared to sand-coating.

As already observed in the tests with EBR systems, the maximum strain in the NSM reinforcement that fail by debonding decreases with the increase of the axial stiffness of the FRP system. Moreover, it was observed that the maximum applicable tensile stress to a given

FRP system is related to the FRP perimeter to area ratio, with best results attained by the carbon strips since they were characterized by the highest values of this shape factor.

The local bond slip relationship for the NSM systems can be approximated by a bilinear diagram, where the shear strength and ultimate slip increases as the axial stiffness of the NSM system is lower and further influenced by the surface texture of the FRP. The elastic stiffness increases as the axial stiffness of the NSM system is greater.

Further numerical investigation is needed in order to assess design formulations for the main parameters of the bond law based on the experimental results collected in the presented RRT and further available in the technical literature.

Acknowledgments

The authors wish to acknowledge the financial assistance of the European Union for the Marie Curie Research Training Network En-Core, and the support of TG 9.3 of the International Federation for Structural Concrete (fib). Hughes Brothers and Fortius, Magmatech, Schock, S&P, Sika and Sto Scandinavia AB are acknowledges for their participation in the RRT and for supplying the test materials.

References

ACI Committee 440 (2008). "Guide Test Methods for Fiber-Reinforced Polymers (FRPs) for Reinforcing or Strengthening Concrete Structures." ACI 440.3R-04, *American Concrete Institute*, 40 pp.

Bilotta A., Ceroni F., Nigro E., Di Ludovico M, Pecce M. and Manfredi G. (2011). "Bond efficiency of EBR and NSM FRP systems for strengthening of concrete members." *Journal of Composites for Construction*, 15(5), 757-772.

Blaschko, M. (2003). "Bond behaviour of CFRP strips glued into slits." *6th Intertnational*

Symposium on FRP Reinforcement for Concrete Structures (FRPRCS-6), Singapore, 205-214.

Ceroni F., Bilotta A., Nigro E and Pecce M. (2012). “Bond Behaviour of FRP NSM systems in concrete elements.” *Composites: Part B*, 43(2), 99-109.

Ceroni F., Barros J. A. O., Pecce M. and Ianniciello M. (2013). “Assessment of non linear bond laws for Near Surface Mounted systems in concrete elements.” *Composites: Part B*, 45(1), 666-681.

Costa, I. G., Barros, J.A.O. (2013). “Critical analysis of fibre-reinforced polymer near-surface mounted double-shear pull-out tests.” *Strain - An International Journal for Experimental Mechanics*, 49, 299-312.

CNR DT 200/R1 (2012) “Guide for the Design and Construction of Externally Bonded FRP Systems for Strengthening Existing Structures.” *Advisory Committee on Technical Recommendation for Construction of National Research council*, Rome, Italy.

De Lorenzis, L., Nanni, A (2001), Characterization of FRP rods as near-surface mounted reinforcement, J of Comp for Construction, 5(2), 114-121.

De Lorenzis, L.,Rizzo, A, La Tegola, A (2002). “A modified pull-out test for bond of near surface mounted FRP rods in concrete.” *Composites Part B: Engineering*, 33(8), 589-603.

De Lorenzis, L., Lundregen K., Rizzo A. (2004). “Anchorage length of near surface mounted FRP bars for concrete strengthening- Experimental investigation and numerical modelling.” *ACI Structural Journal,* 101(2), 269-278.

De Lorenzis L., Teng, J.G. (2007). Near-surface mounted FRP reinforcement: an emerging technique for structural strengthening, Composites: Part B, Vol. 38, pp. 119–143.

Guadagnini M., Serbescu A., Palmieri A., Matthys S., Bilotta A., Nigro E., Ceroni F., Czaderski

C., Olia S., Szabo Z., Balazs G. and Mazzotti C. (2012). “Round Robin Test on the bond behavior of externally bonded FRP systems to concrete.” *6th International Conference on FRP Composites in Civil Engineering* (CICE2012), Rome, Italy, CD ROM.

Hassan T. and Rizkalla S. (2003). “Investigation of bond concrete structures strengthened with near surface mounted carbon fiber reinforced polymer strips.” *Journal of Composites for Construction,* 7(3), 248-257.

Horiguchi, T. and Saeki, N. (1997), Effect of Test Methods and Quality of Concrete on Bond strength of CFRP sheet, Non-Metallic (FRP) Reinforcement for Concrete Structures, Japan Concrete Institute, 265-270.

ISO TC 71/SC 6 N (2003). “Non-conventional reinforcement of concrete - Test methods - Part 1: Fiber reinforced polymer (FRP) bars and grids.” *International Organization for Standardization*, 48 pp.

Kotynia R. (2005). “Strain Efficiency of Near Surface Mounted CFRP-strengthened Reinforced Concrete Beams.” T*hird International Conference on Composites in Construction* (CCC 2005), Lyon.

Sena-Cruz, J.M.; Barros, J.A.O., (2004). Bond Between Near-Surface Mounted Carbon-Fiber-Reinforced Polymer Laminate Strips and Concrete. *Journal of Composites for Construction, ASCE*, 8(6), 519-527, 2004.

Seracino, R; Jones, NM; Ali, SM; Page, MW; Oehlers, DJ, (2007) Bond strength of near-surface mounted FRP strip-to-concrete joints. *Journal of Composites for Construction*, *ASCE*, 11(4), 401-409, 2007.

Seracino R., Saifulnaz M. R., Oehlers D. J. (2007). “Generic Debonding Resistance of EB and NSM Plate-to Concrete Joints”, *Journal of Composites for Construction,* 11(1), 62-70.

Ueda, T., Dai, J.G. (2005), Interface of Fiber Reinforced Polymer Laminates Externally Bonded to Concrete Substrate: from Test Methods to Bond Modelling, Proceedings of the

International Symposium on Bond Behaviour of FRP in Structures (BBFS 2005), 23-34.

Table 1. Summary of main procedural differences between testing laboratories.

Lab.	Test	Loading rate [mm/min]	Embedded bars n°/diam. [mm]	Concrete properties at 28d				Concrete properties at age of testing			
				$f_{cm,cyl}$	$f_{cm,cub}$	$f_{ctm,flex}$	E_c	$f_{cm,cyl}$	$f_{cm,cub}$	$f_{ctm,flex}$	E_c
				[MPa]			[GPa]	[MPa]			[GPa]
Ghent	DB	0.10	2/16	29.7	34.2	3.8	27.6	-	-	-	-
Minho	DB	0.50	2/16	26.4	-	3.31	24.4	35.1	-	3.7	25.8
Naples/Sannio	SB	0.18	2/20	19.6	-	-	18.6	-	23.1	-	-
Budapest	DB	0.10	1/22	-	49.3	3.9	-	-	51.9	4.0	-

Table 2. Test matrix.

Specimens	Fibers	Surface	Dimension[1] [mm]	Groove dimensions [mm]			
				Naples Sannio	Ghent	Minho	Budapest
C_SC_6	Carbon	Sand coated bar	6	-	12x12	10x12	12x12
B_SC_6	Basalt	Sand Coated bar	6	10x10	12x12	9.5x10	12x12
B_SC_8	Basalt	Sand Coated bar	8	14x14	14x14	12x12	14x14
C_S_1.4x10	Carbon	Smooth strip	1.4x10	5x15	5x15	5x15	5x15
G_RB_8	Glass	Ribbed bar	10	14x14	14x14	12x12	14x14
C_S_2.5x15	Carbon	Smooth strip	2.5x15	8x25	8x25	8x24	8x25
C_S_8	Carbon	Smooth bar	8	14x14	14x14	13x13	14x14
C_S_10x10	Carbon	Smooth square bar	10x10	15x15	15x15	15x16	15x15
G_SW_8	Glass	Spirally wounded bar	8	14x14	14x14	-	14x14

[1] The bar diameter and strip dimensions are nominal

Table 3. NSM FRP properties obtained by each laboratory

Specimens	Naples & Sannio		Ghent		Minho	
	f_u [MPa]	E_f [GPa]	f_u [MPa]	E_f [GPa]	f_u [MPa]	E_f [GPa]
C_SC_6	-	-	2885 (9%)	162 (2%)	3536 (6%)	187 (2%)
B_SC_6	1282 (8%)	46 (3%)	1413 (8%)	52 (4%)	1715 (4%)	54 (1%)
B_SC_8	1272 (7%)	46 (3%)	1208 (13%)	48 (9%)	1493 (5%)	53 (1%)
C_S_1.4x10	2221 (9%)	177 (3%)	2756 (7%)	171 (1%)	3047 (2%)	175 (1%)
G_RB_8	1333 (4%)	59 (7%)	1230 (21%)	59 (4%)	1776 (3%)	65 (3%)
C_S_2.5x15	2863 (5%)	182 (1%)	1558 (13%)	178 (5%)	1813 (11%)	171 (1%)
C_S_8	2495 (3%)	155 (1%)	-	-	-	157 (5%)
C_S_10x10	1397 (7%)	159 (6%)	1360 (4%)	180 (11%)	1505 (17%)	179 (2%)
G_SW_8	1250 (5%)	51 (5%)	1352 (7%)	53 (5%)	-	-

Table 4. Average NSM FRP Properties

Specimens	Exp. Average values& COV		Manufacturer's data		$f_{u,exp}/f_{u,nom}$	$E_{f,exp}/E_{f,nom}$	A_f[1] [mm^2]	E_f Af [MN]
	$f_{u,exp}$ [MPa]	$E_{f,exp}$ [GPa]	$f_{u,nom}$ [MPa]	$E_{f,nom}$ [GPa]				
C_SC_6	3211 (14%)	175 (10%)	2068	124	1.55	1.41	29.9	5218
B_SC_6	1470 (15%)	51 (8%)	-	50	-	1.02	29.9	1515
B_SC_8	1324 (11%)	49 (7%)	-	50	-	0.98	50.2	2460
C_S_1.4x10	2675 (16%)	174 (2%)	1850	165	1.45	1.05	14.0	2441
G_RB_8	1443 (20%)	61 (6%)	1500	60	0.96	1.02	50.0	3050
C_S_2.5x15	2078 (33%)	177 (3%)	3100	165	0.67	1.07	37.5	6638
C_S_8	2495 (3%)	156 (1%)	2800	155	0.89	1.00	50.2	7831
C_S_10x10	1421 (5%)	173 (7%)	2000	155	0.71	1.12	100.0	17300
G_SW_8	1301 (6%)	52 (3%)	-	-	-	-	50.2	2610

[1] *the cross-sectional area is nominal*

Table 5. Properties of the adhesive

Adhesive Type	Samples	Manufacturer		E_a [GPa]			f_a [MPa]		
		E_a [GPa]	f_a [MPa]						
Fortresin CFL	6	-	50	8.87	(0.38)	{4%}	21.7	(6.8)	{31%}
Sikadur-30	6	12.8	30	10.7	(0.3)	{3%}	33.7	(0.9)	{3%}
StoPox SK 41	6		-	7.61	(0.66)	{9%}	20.3	(1.8)	{9%}

Average (Standard deviation) {Coefficient of variation}

Table 6. Failure load for the NSM reinforcements in the case of debonding failure

	Gent						Minho					
	F_u [kN]	F_u [kN]	F_u [kN]	$F_{u,av}$ [kN]	CoV [%]	FA	F_u [kN]	F_u [kN]	F_u [kN]	$F_{u,av}$ [kN]	CoV [%]	FA
C_SC_6	31.5	30.6	36.8	**33.0**	10	2	38.7	33.0	38.3	**36.7**	9	3
B_SC_6	26.7	30.8	27.7	**28.4**	8	3	23.0	25.1	31.4	**26.5**	16	2
B_SC_8	46.1	37.6	35.8	**39.8**	14	3	31.0	37.1	32.3	**33.5**	10	2
C_S_1.4x10	-	-	-	**-**	-	-	36.6	39.4	41.4	**39.1**	6	2
G_RB_8	55.6	56.3	43.3	**51.7**	14	3	38.6	38.6	43.8	**40.3**	7	2
C_S_2.5x15	-	-	-	**-**	-	-	49.6	48.3	48.0	**48.6**	2	2
C_S_8	56.8	51.4	62.5	**56.9**	14	1	47.5	49.0	45.8	**47.4**	3	2
C_S_10x10	65.1	59.6	-	**62.4**	6	2	-	-	-	**-**	-	-
G_SW_8	43.3	43.2	44.6	**47.7**	2	2	-	-	-	**-**	-	-

Failure aspects:
1. Debonding at the FRP-adhesive interface (DB-FRP/A)
2. Debonding at the concrete-adhesive interface, with various degrees of concrete damage (DB-C/A)
3. Adhesive splitting failure (SP-A)

Table 7. Failure load for the NSM reinforcements in the case of debonding failure

	Naples/Sannio						Budapest					
	F_u [kN]	F_u [kN]	F_u [kN]	$F_{u,av}$ [kN]	CoV [%]	FA	F_u [kN]	F_u [kN]	F_u [kN]	$F_{u,av}$ [kN]	CoV [%]	FA
C_SC_6	-	-	-	**-**	-		33.2	34.5	-	**33.9**	3	3
B_SC_6	33.9	28.8	-	**31.4**	11	2						
B_SC_8	31.6	33.1	30.2	**31.6**	5	2	28.5	32.7	-	**30.6**	10	2
C_S_1.4x10	-	-	-	**-**	-	-						
G_RB_8	46.7	45.3	50.9	**47.6**	6	2	45.8	43.5	-	**44.7**	4	3
C_S_2.5x15	53.0	56.0	46.3	**51.8**	10	2	39.7	41.0	40.6	**40.4**	2	2
C_S_8	48.5	55.3	45.2	**49.7**	10	2	40.7	41.5	42.7	**41.6**	2	2/3
C_S_10x10	51.7	47.9	51.6	**50.4**	4	2	-	-	-	**-**	-	-
G_SW_8	40.8	38-0	-	**39.4**	5	1	-	-	-	**-**	-	-

Failure aspects:
4. Debonding at the FRP-adhesive interface (DB-FRP/A)
5. Debonding at the concrete-adhesive interface, with various degrees of concrete damage (DB-C/A)
6. Adhesive splitting failure (SP-A)

Table 8. Average failure loads and stresses for the NSM reinforcements in the case of debonding failure

Specimens	Average values			
	$F_{u,av}$ [kN]	CoV [%]	τ_{av} [MPa]	σ_{max} [MPa]
C_SC_6	**34.5**	6	6.1	1154
B_SC_6	**28.8**	9	5.1	962
B_SC_8	**33.9**	12	4.5	675
C_S_1.4x10	**39.1**	-	5.7	2795
G_RB_8	**46.1**	10	6.1	922
C_S_2.5x15	**46.9**	12	4.5	1252
C_S_8	**48.9**	13	6.5	974
C_S_10x10	**56.4**	15	4.7	564

G_SW_8	**41.6**	7	5.5	828

Table 9. Failure load for the NSM reinforcements in the case of concrete failure (SP-C)

Specimen	Ghent					Minho					Budapest					Average
	F_u [kN]			$F_{u,av}$ [kN]	CoV [%]	F_u [kN]			$F_{u,av}$ [kN]	CoV [%]	F_u [kN]			$F_{u,av}$ [kN]	CoV [%]	$F_{u,av}$ [kN]
C_S_1.4x10	25.0	24.3	-	**24.7**	4	-	-	-	**-**	-	25.4	23.9	26.0	**25.1**	4	**24.9**
C_S_2.5x15	60.6	60.9	58.1	**59.9**	3	-	-	-	**-**	-	-	-	-	**-**	-	**59.9**
C_S_10x10	-	-	58.2	**58.2**	-	62.7	59.0	55.0	**58.9**	7	59.7	56.9	-	**58.3**	3	**58.5**

Table 10. Failure load for the NSM reinforcements in the case of tensile failure of fibres (T-FRP)

Specimens	Naples/ Sannio				
	F_u [kN]			$F_{u,av}$ [kN]	CoV [%]
C_S_1.4x10	31.2	33.0	34.7	**32.9**	5
B_SC_6	-	-	36.3	**36.3**	-

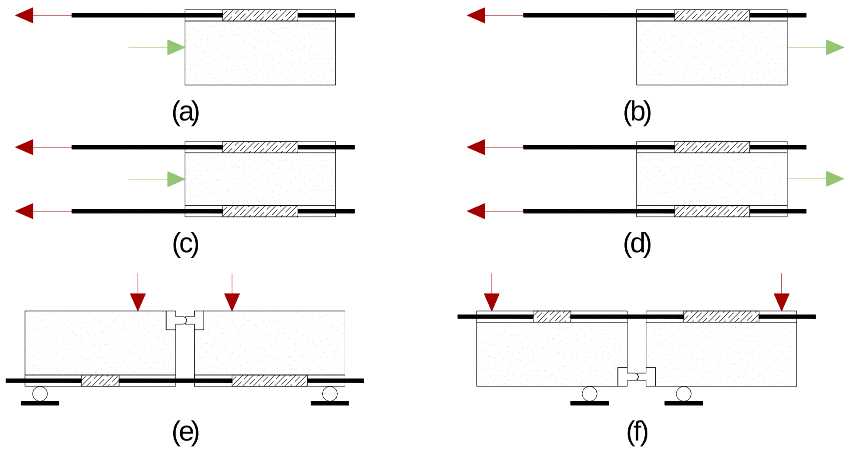

Figure 1. Test setups for assessing the NSM FRP bond behaviour: (a) Single-Shear Pushing Test, (b) Single-Shear Pulling Test, (c) Double-Shear Pushing Test,(d) Double-Shear Pulling Test and (e-f) Beam Bending Test.

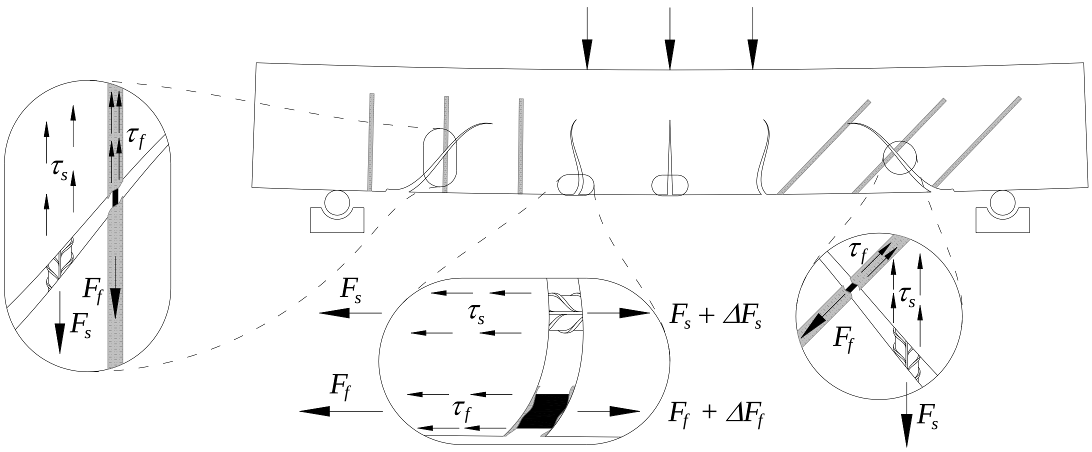

Figure2. Conceptual representation of the stress field introduced by the reinforcements in the surrounding concrete in real FRP strengthened elements.

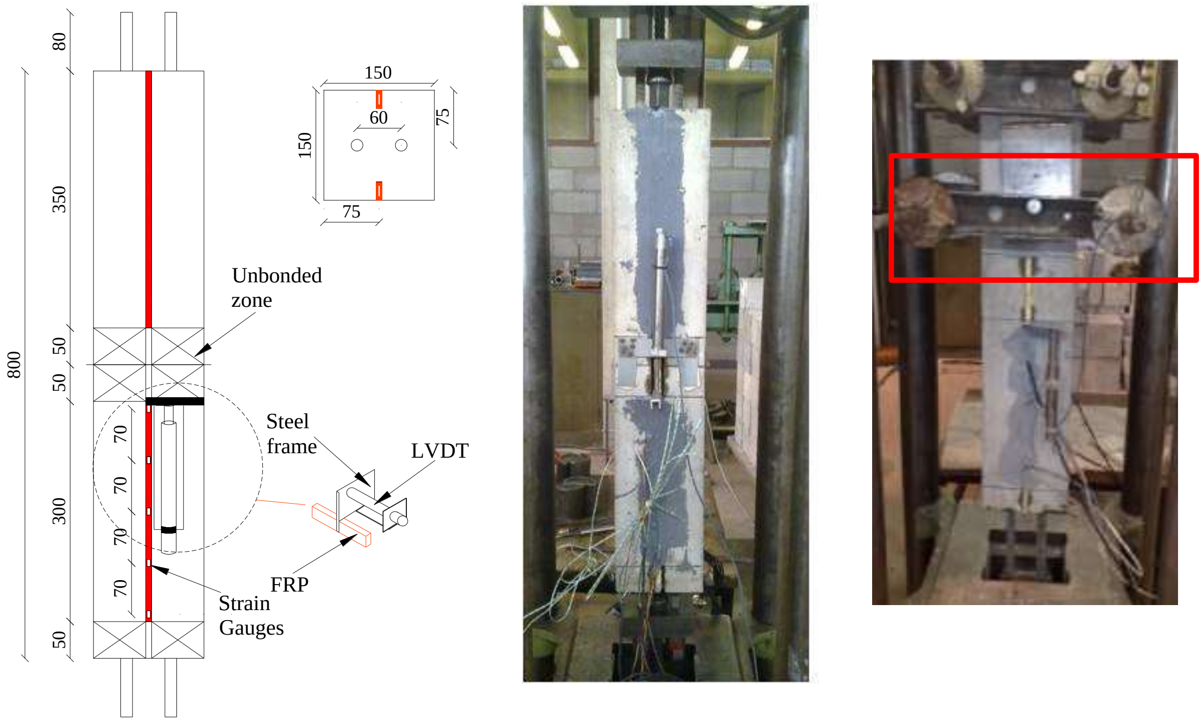

a1) a2) a3)

Figure 3a. DB test set-up of Gent Laboratory: a1) specimen and instrumentation details; a2) specimen in the testing machine; a3) detail of extra mechanical anchoring system.

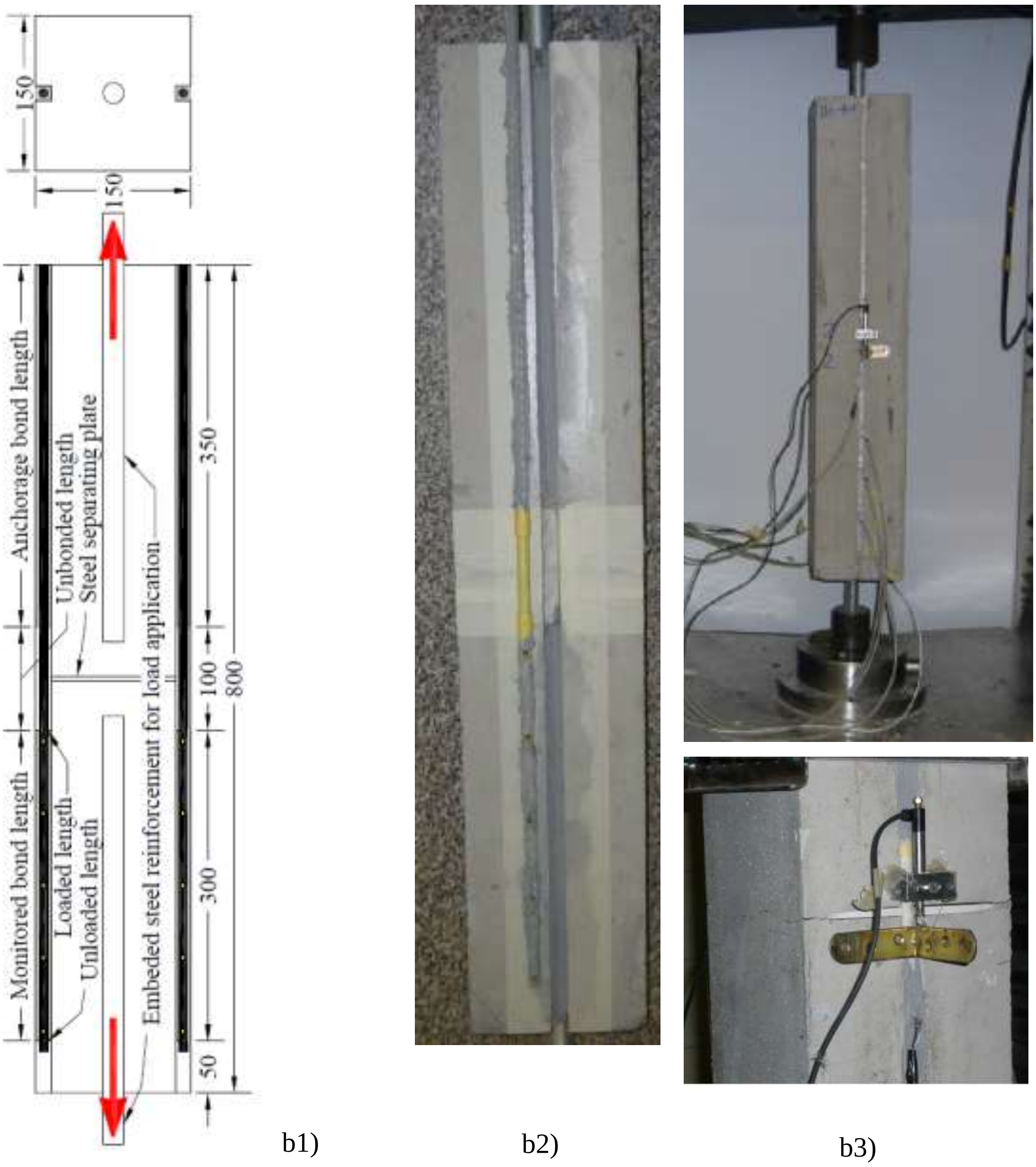

b1) b2) b3)

Figure 3b. DB test set-up of Budapest Laboratory: b1) specimen details; b2) position of strain gauges along the NSM reinforcement spaced of 70 mm; b3) specimen in the testing machine and detail of LVDT.

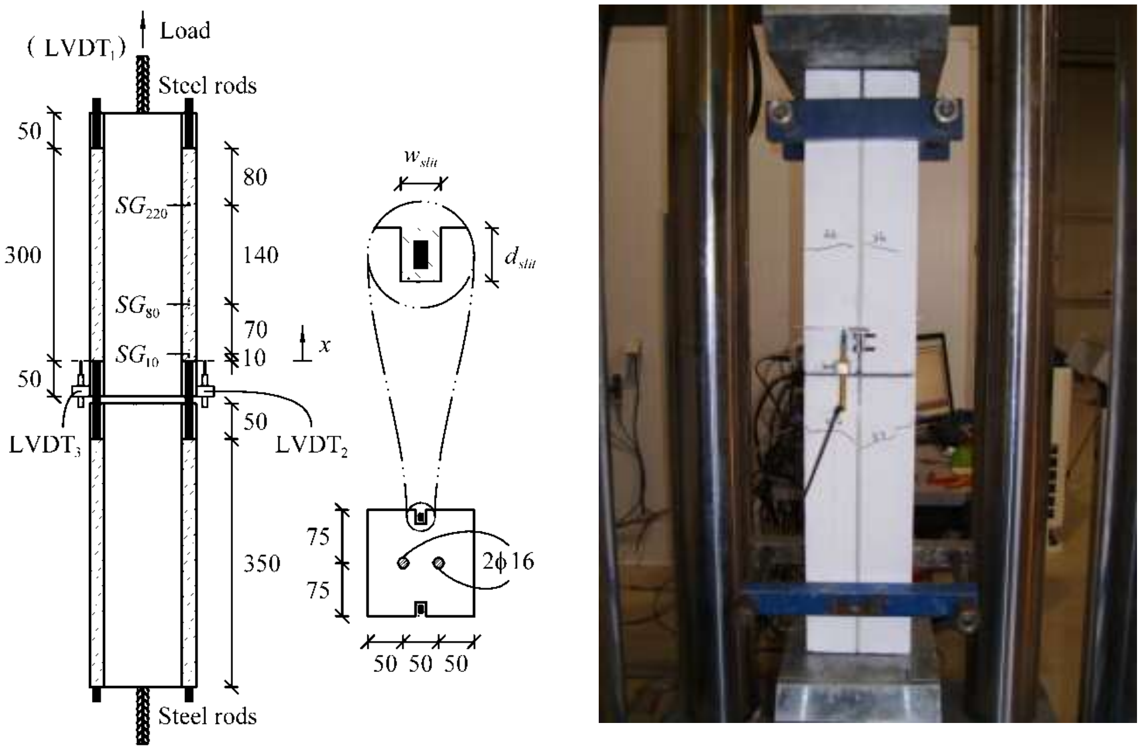

c1) c2)

Figure 3c. DB test set-up of Minho Laboratory: c1) specimen and instrumentation details; c2) detail of extra mechanical anchoring system and of LVDTs.

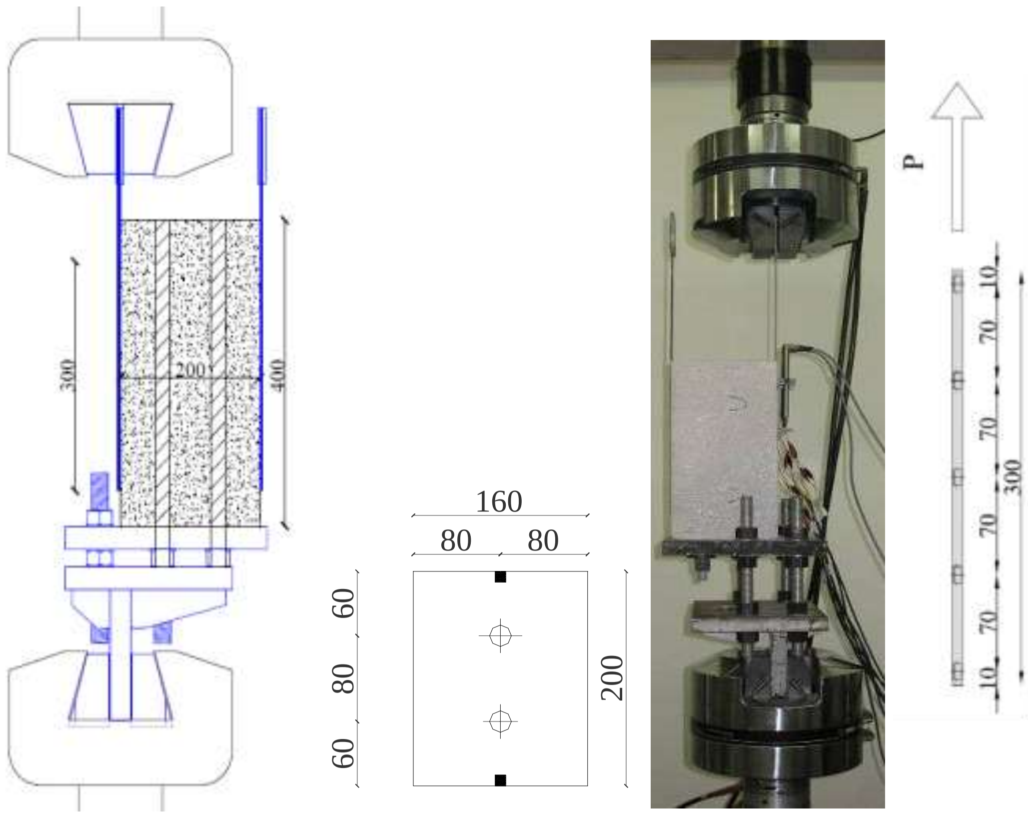

d1) d2) d3)

Figure 3d. SB test set-up of Naples/Sannio Laboratory: d1) specimen details; d2) specimen in the testing machine; d3) position of strain gauges along the NSM FRP reinforcement.

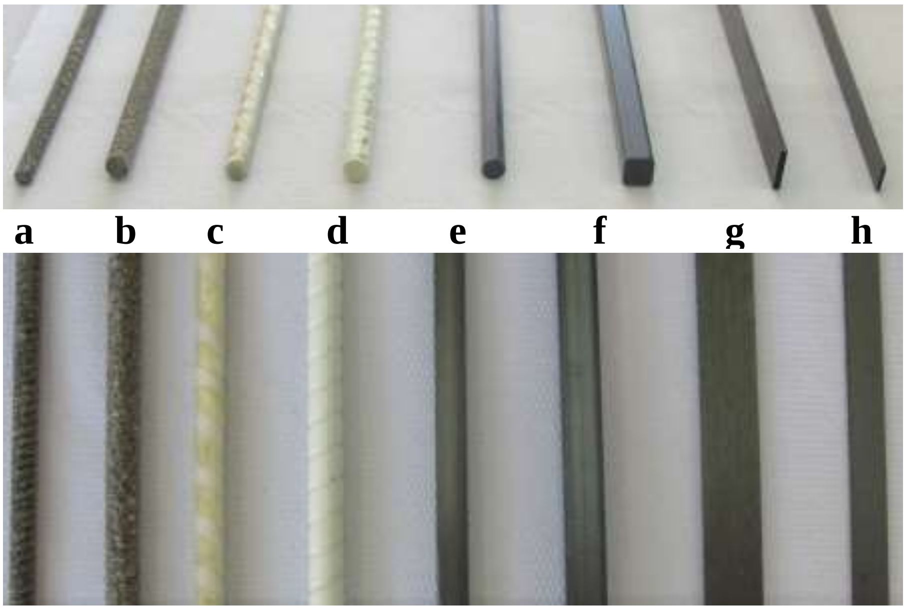

Figure 4. Bar surface configuration: a, b) sand-coated basalt round bar; c) spirally wound round glass bars; d) ribbed round glass bars; e) smooth round carbon bars; f) smooth square carbon bars; g-h) smooth carbon strips.

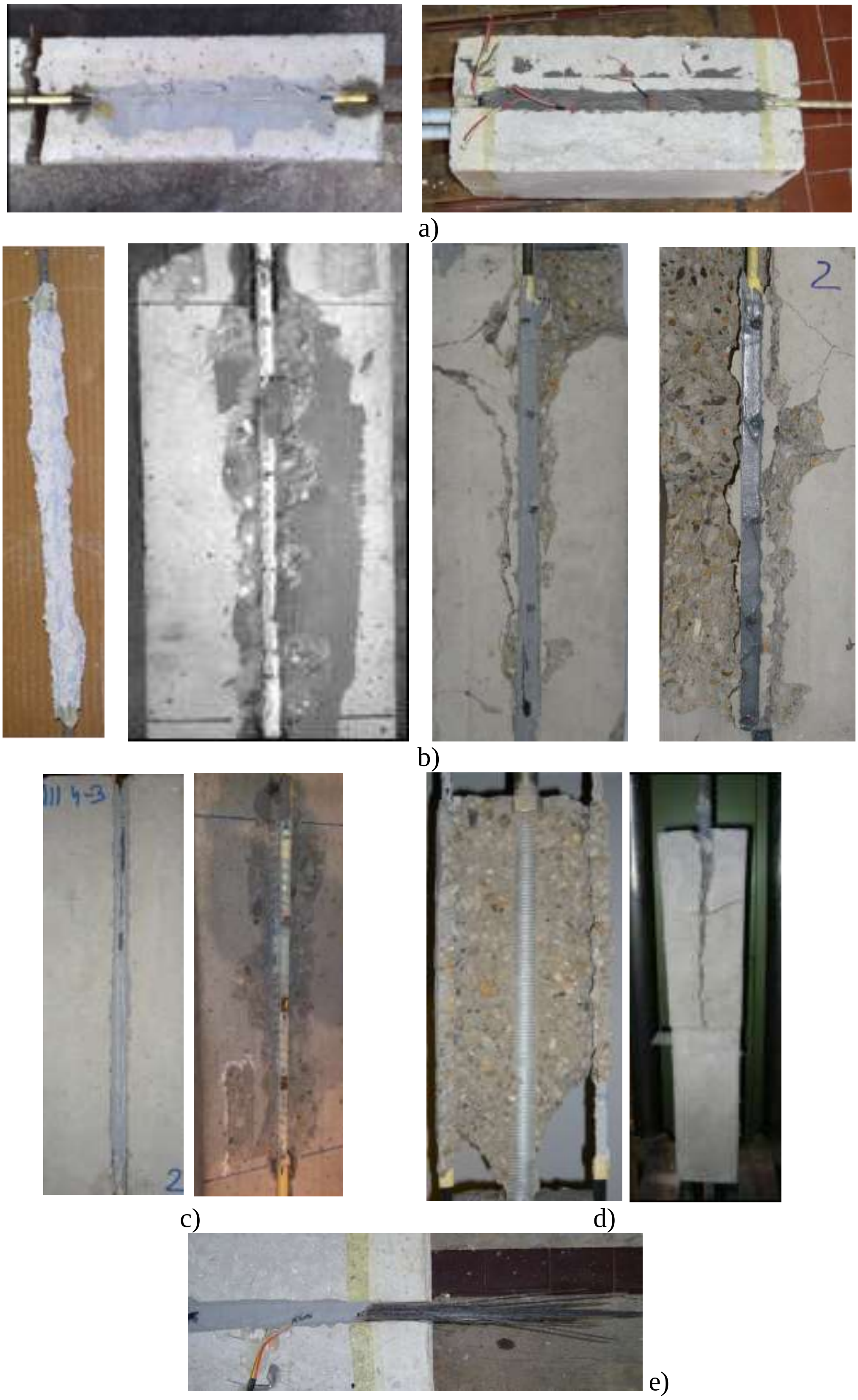

Figure 5. Examples of experimentally observed failure aspects: a) Debonding at the FRP-adhesive interface (DB-FRP/A); b) Debonding at the concrete-adhesive interface, with various degrees of concrete damage (DB-C/A); c) Adhesive splitting failure (SP-A); d) Splitting failure of the concrete along the plane of the internal steel bars (SP-C); e) Tensile failure of the FRP (T-FRP).

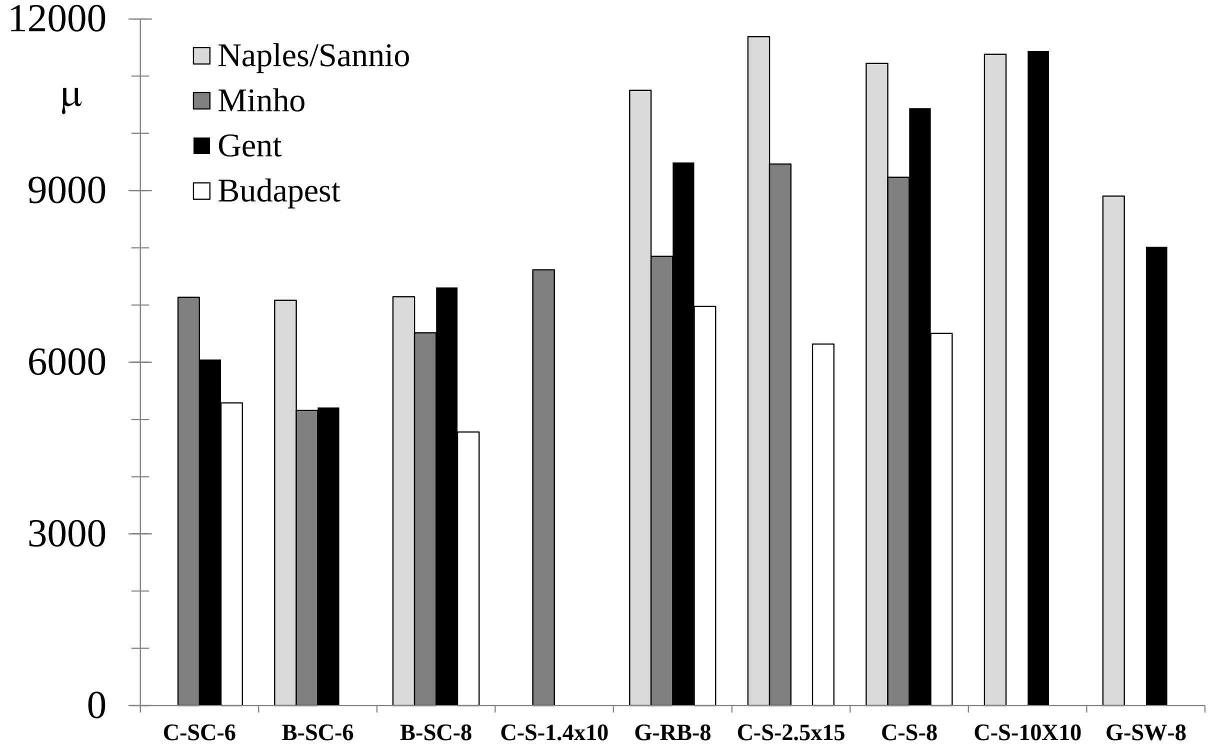

Figure 6. Normalized average maximum load.

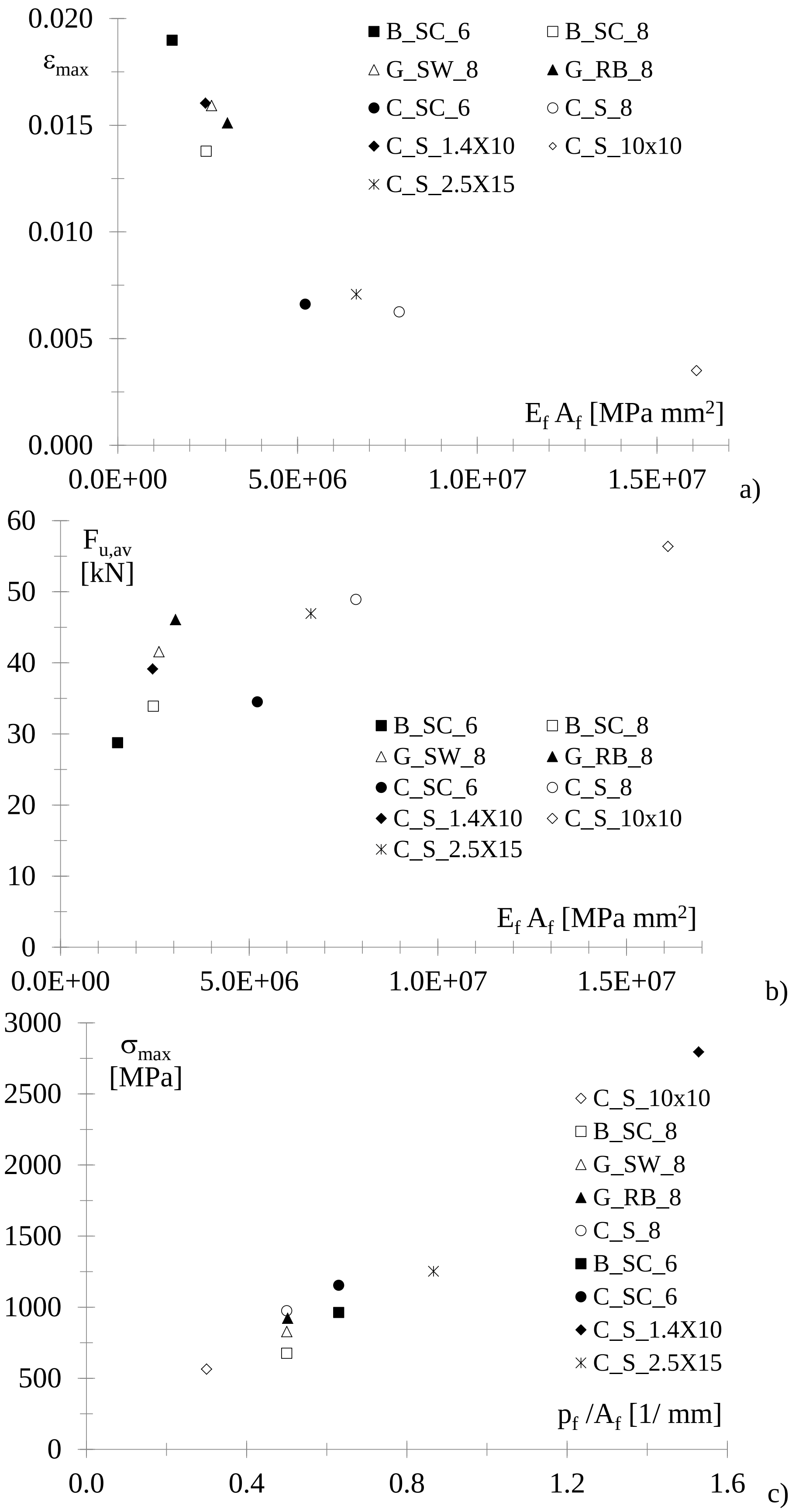

Figure 7. a) Average maximum strain versus axial stiffness, b) Maximum load versus axial stiffness and c) Maximum tensile stress vs. NSM perimeter/area ratio.

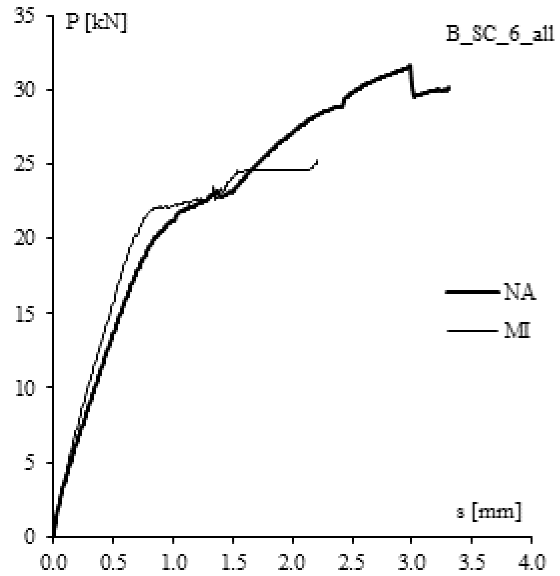
P [kN]
B_SC_6_all
NA
MI
s [mm]
0
5
10
15
20
25
30
35
0.0
0.5
1.0
1.5
2.0
2.5
3.0
3.5
4.0

a)

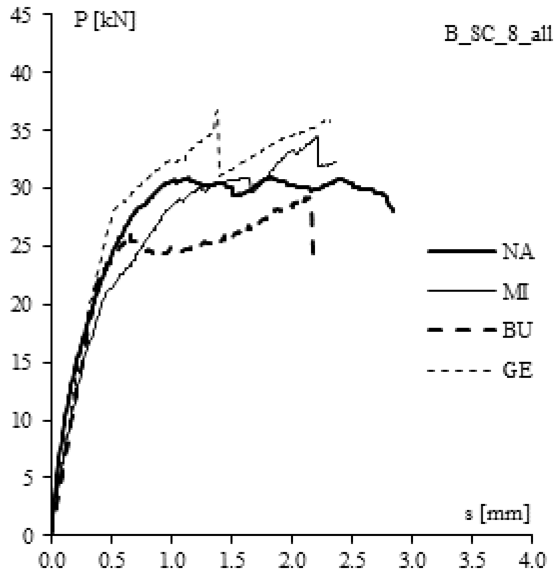
P [kN]
B_SC_8_all
NA
MI
BU
GE
s [mm]
0
5
10
15
20
25
30
35
40
45
0.0
0.5
1.0
1.5
2.0
2.5
3.0
3.5
4.0

b)

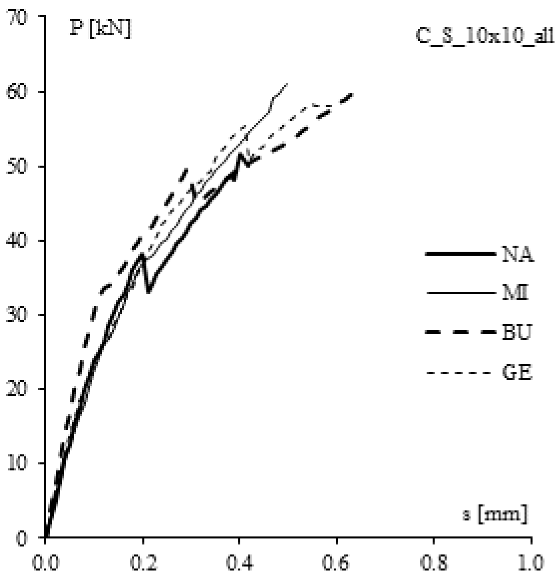
P [kN]
C_S_10x10_all
NA
MI
BU
GE
s [mm]
0
10
20
30
40
50
60
70
0.0
0.2
0.4
0.6
0.8
1.0

c)

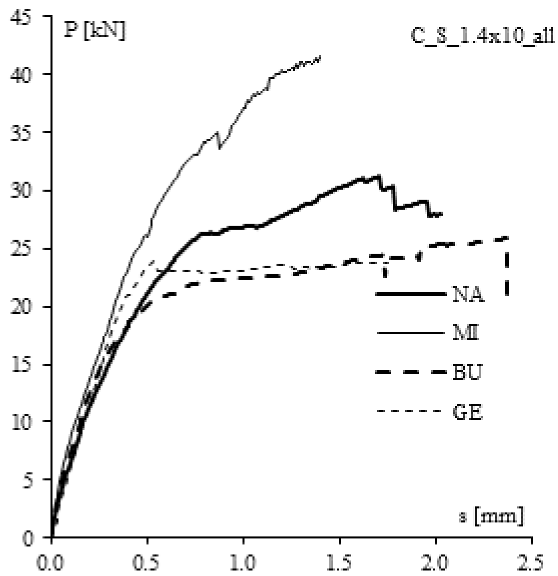
P [kN]
C_S_1.4x10_all
NA
MI
BU
GE
s [mm]
0
5
10
15
20
25
30
35
40
45
0.0
0.5
1.0
1.5
2.0
2.5

d)

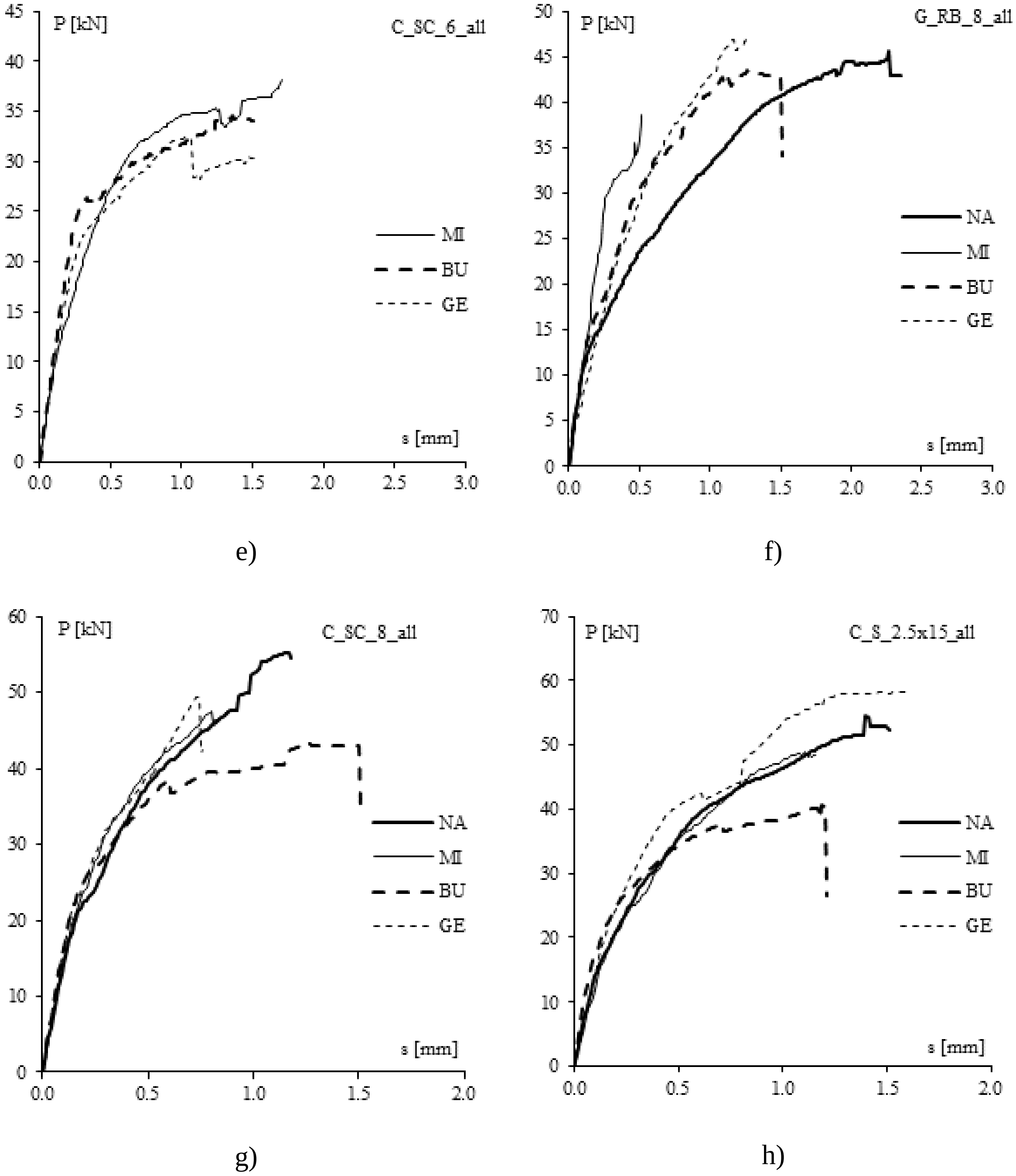

Figure 8. Load displacement curves

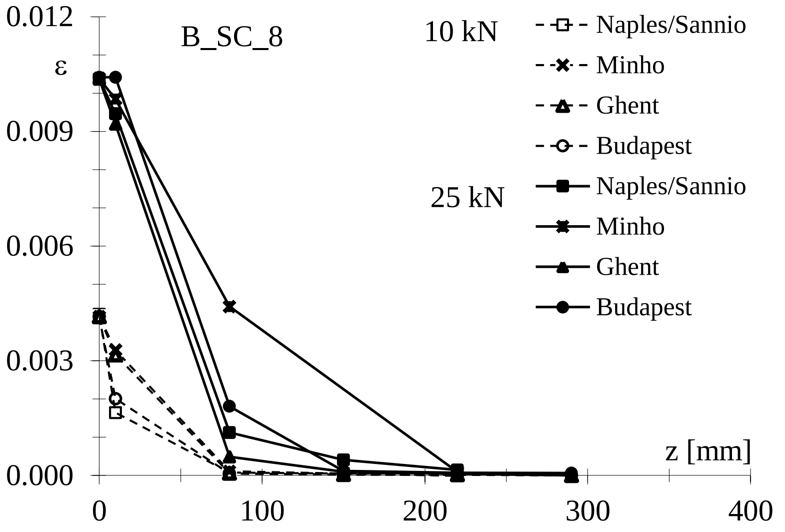
B_SC_8
ε
z [mm]
10 kN
Naples/Sannio
Minho
Ghent
Budapest
25 kN
Naples/Sannio
Minho
Ghent
Budapest
0.012
0.009
0.006
0.003
0.000
0
100
200
300
400
a)

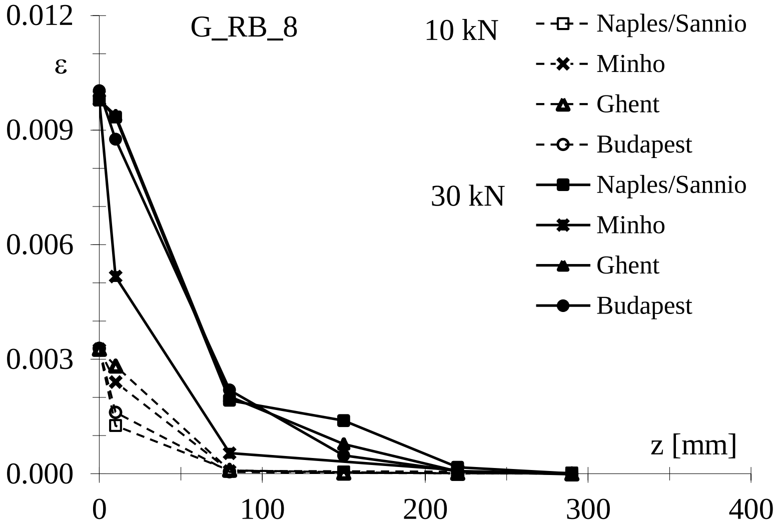
G_RB_8
ε
z [mm]
10 kN
Naples/Sannio
Minho
Ghent
Budapest
30 kN
Naples/Sannio
Minho
Ghent
Budapest
0.012
0.009
0.006
0.003
0.000
0
100
200
300
400
b)

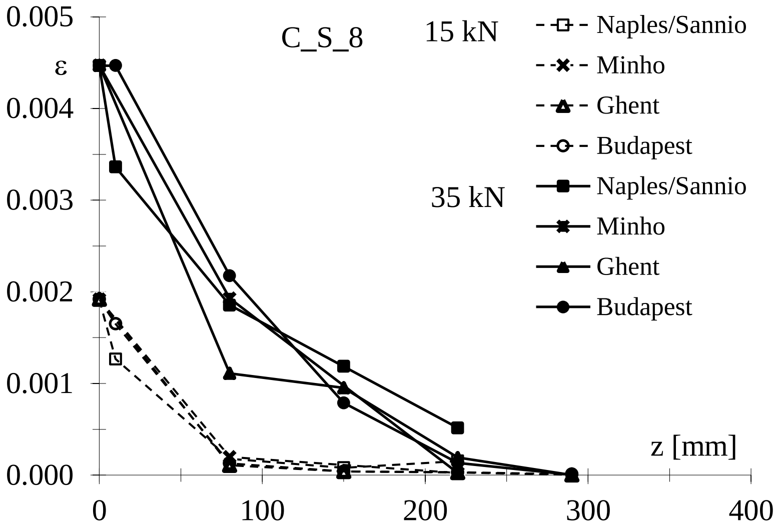
C_S_8
ε
z [mm]
15 kN
Naples/Sannio
Minho
Ghent
Budapest
35 kN
Naples/Sannio
Minho
Ghent
Budapest
0.005
0.004
0.003
0.002
0.001
0.000
0
100
200
300
400
c)

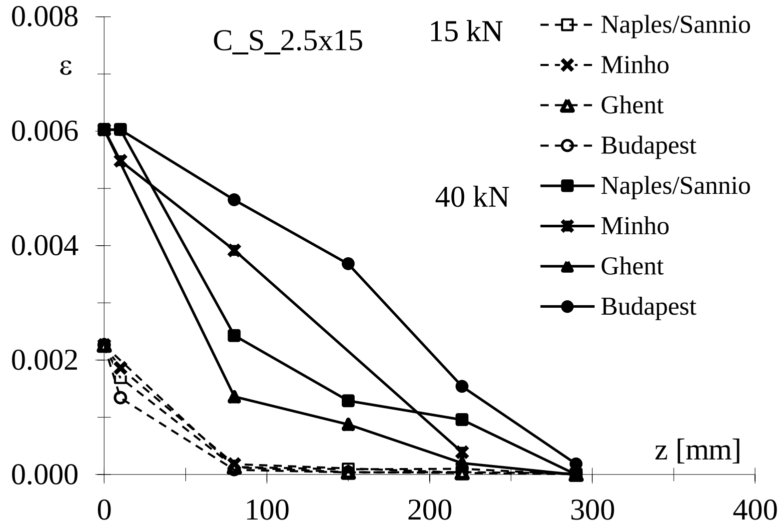

C_S_2.5x15
15 kN
40 kN
ε
Naples/Sannio
Minho
Ghent
Budapest
Naples/Sannio
Minho
Ghent
Budapest
z [mm]
0.008
0.006
0.004
0.002
0.000
0
100
200
300
400

d)

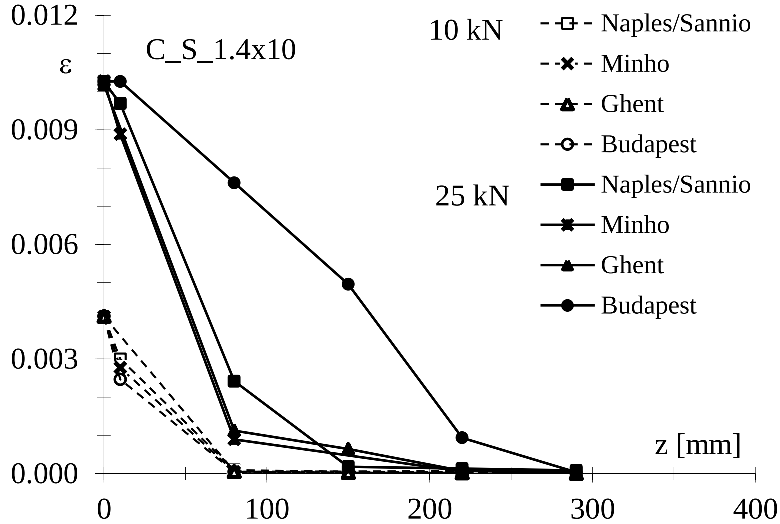

C_S_1.4x10
10 kN
25 kN
ε
Naples/Sannio
Minho
Ghent
Budapest
Naples/Sannio
Minho
Ghent
Budapest
z [mm]
0.012
0.009
0.006
0.003
0.000
0
100
200
300
400

e)

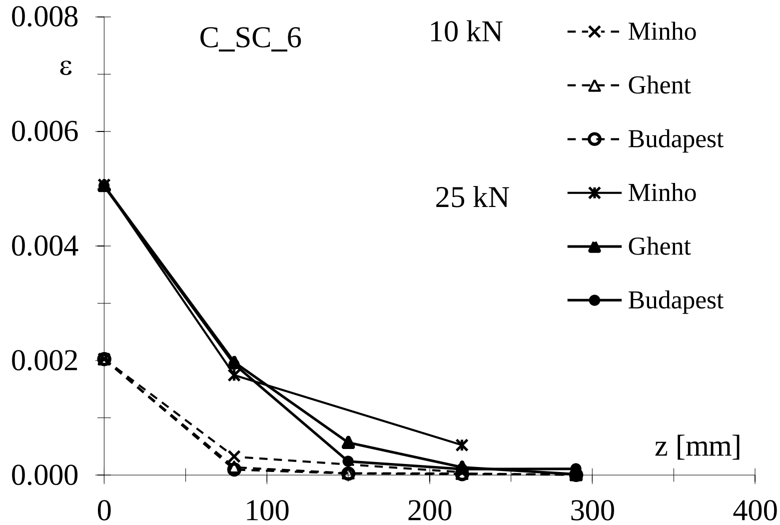

C_SC_6
10 kN
25 kN
ε
Minho
Ghent
Budapest
Minho
Ghent
Budapest
z [mm]
0.008
0.006
0.004
0.002
0.000
0
100
200
300
400

f)

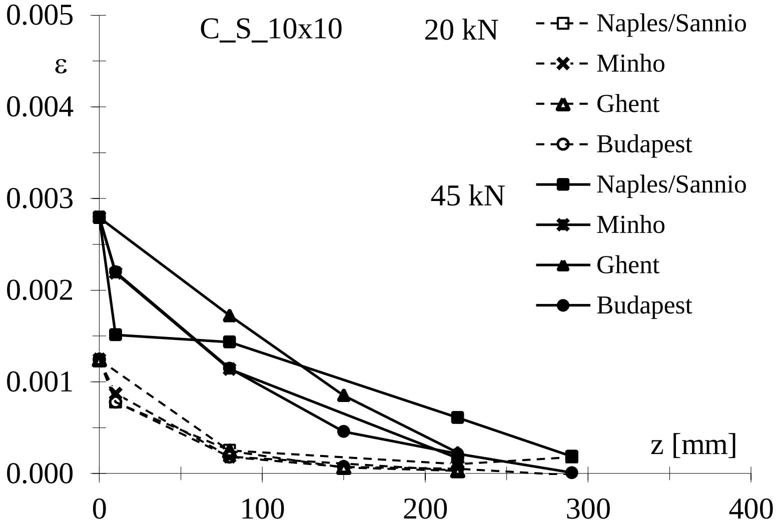

g)

Figure 9. Strain distribution

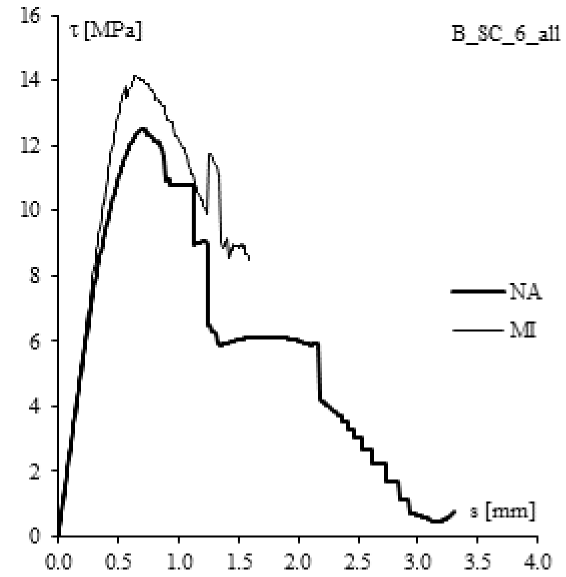
τ [MPa]
B_SC_6_all
NA
MI
s [mm]

a)

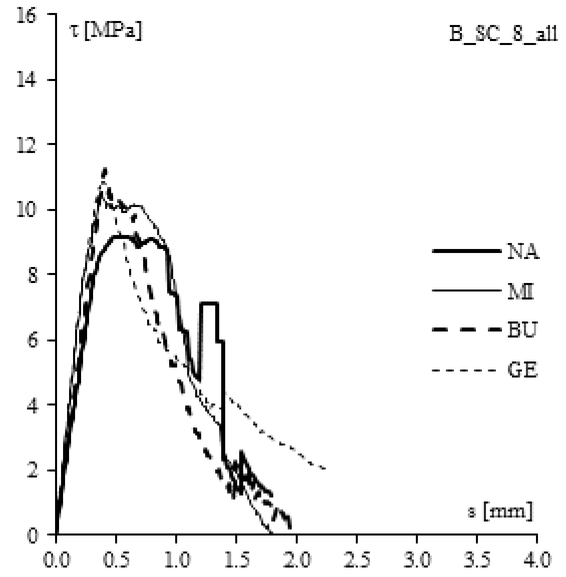
τ [MPa]
B_SC_8_all
NA
MI
BU
GE
s [mm]

b)

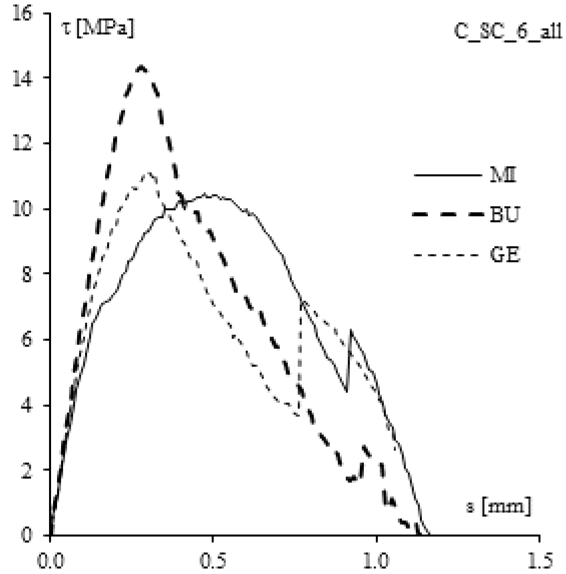
τ [MPa]
C_SC_6_all
MI
BU
GE
s [mm]

c)

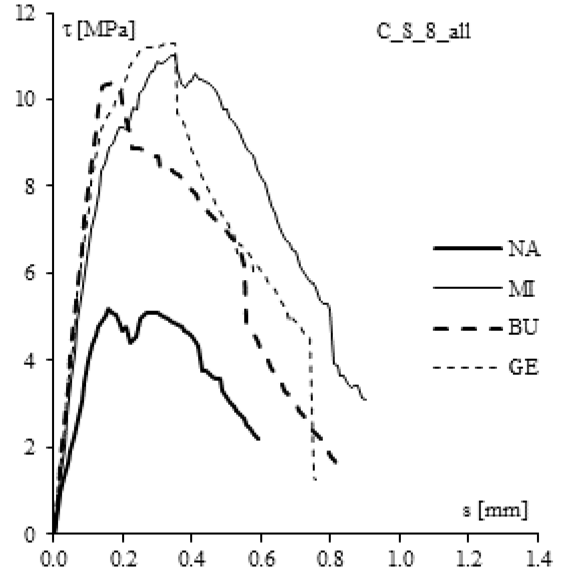
τ [MPa]
C_S_8_all
NA
MI
BU
GE
s [mm]

d)

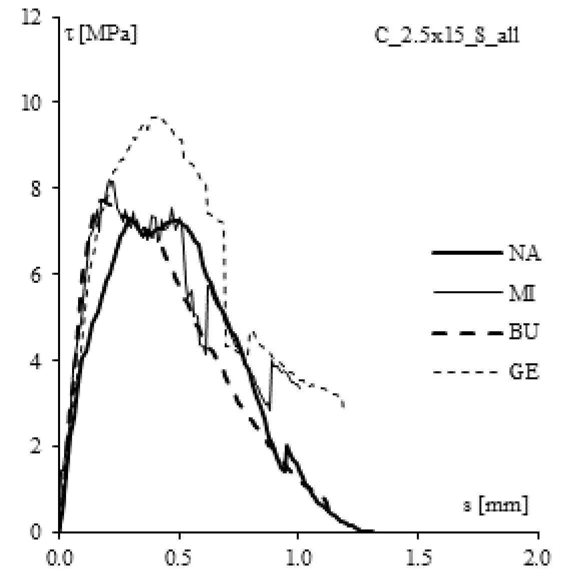
τ [MPa]
C_2.5x15_S_all
NA
MI
BU
GE
s [mm]

e)

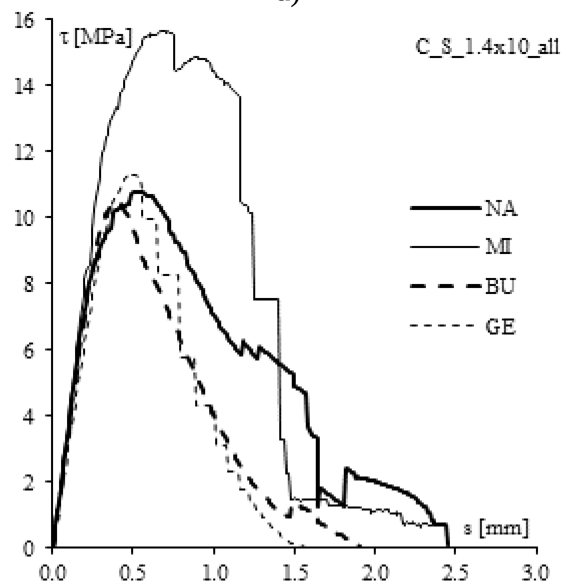
τ [MPa]
C_S_1.4x10_all
NA
MI
BU
GE
s [mm]

f)

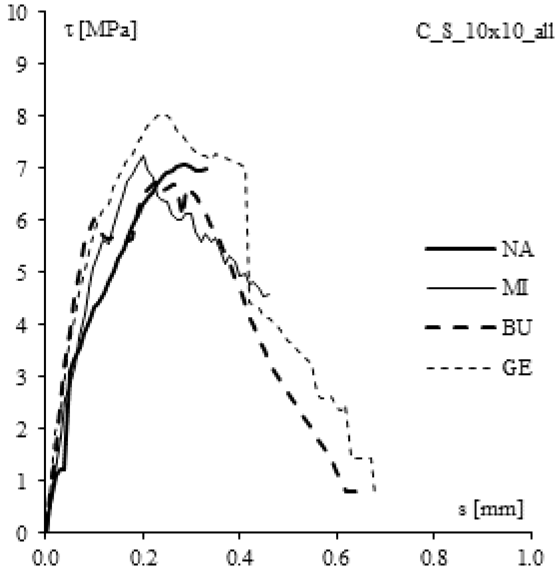

g)

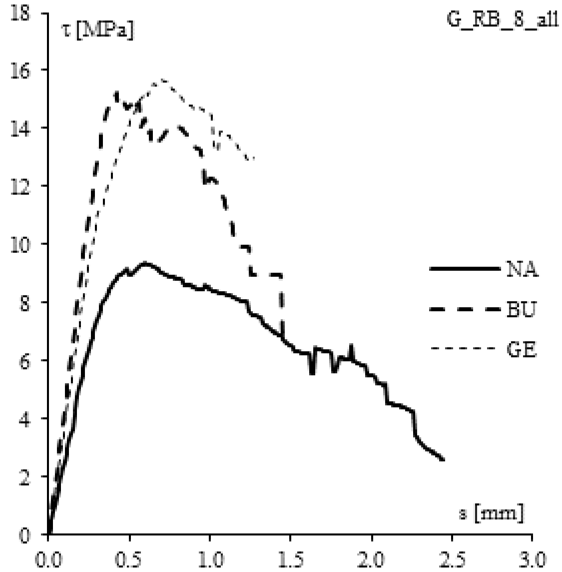

h)

Figure 10. Average bond-slip relationships.

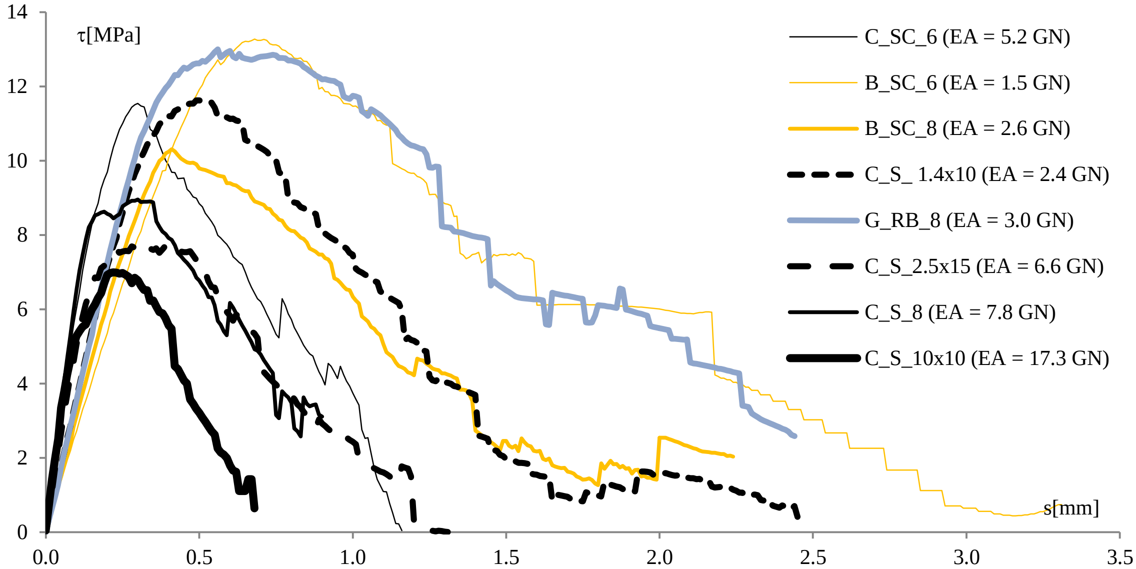

Figure 11. Experimental average local bond-slip relationship.